A Pulsed and Continuous Wave 250 MHz Electron Paramagnetic Resonance Spectrometer

RICHARD W. QUINE,[1] GEORGE A. RINARD,[1] SANDRA S. EATON,[2] GARETH R. EATON[2]

[1]*Department of Engineering and* [2]*Department of Chemistry and Biochemistry, University of Denver, Denver, Colorado* 80208-2436

ABSTRACT: A 250 MHz electron paramagnetic resonance (EPR) spectrometer was constructed to be an engineering test facility for in vivo EPR imaging of physiological samples and for protein structure determination. Innovations relative to prior low-frequency EPR spectrometers include a four-coil, air-core magnet and gradient coils, a crossed-loop resonator, dynamic *Q*-switching to decrease dead time in pulsed EPR, and a narrow-band bridge based on circulators. The automatic frequency control system uses a signal separate from the EPR signal to make the frequency control independent of the radiofrequency (RF) phase. The design incorporates multiple excitation and signal paths to facilitate testing of a variety of resonators, two magnets, and both a locally built console described here and a Bruker console. Plug-in cards in the bridge facilitate using reflection or crossed-loop resonators in continuous wave or pulsed EPR modes. In the locally built console there is a microprocessor-controlled interface unit to handle magnetic field modulation and scan, tuning display, and other functions. Concepts in Magnetic Resonance (Magn Reson Engineering) 15: 59–91, 2002.

KEY WORDS: EPR; imaging; spectrometer design; pulsed EPR

INTRODUCTION

Electron paramagnetic resonance (EPR) in the tens to hundreds of megahertz range has been performed in many laboratories, beginning with the discovery of EPR (*1*). The majority of EPR spectra are obtained at X-band (~9 GHz). There are many incentives for obtaining EPR spectra at frequencies below X-band. Resonator structures can be made to accommodate larger samples (e.g., mice) at lower frequencies. The tradeoffs between sample volume, resonator filling factor, and microwave loss factor can be optimized at frequencies below X-band for some lossy samples, including biological (aqueous) samples. The tradeoffs between g-anisotropy and a-anisotropy can result in the minimum linewidth and hence the best hyperfine resolution occurring at frequencies below X-band. Some electron spin relaxation mechanisms are magnetic field dependent (*2*). Measurements of relaxation times at a wide range of magnetic fields are needed to provide a test of mechanism. Swartz and Halpern (*3*) recently reviewed in vivo EPR comprehensively, covering the low-frequency literature; Greenslade et al. (*4*) critically reviewed low-frequency EPR and discussed the relative benefits of various approaches.

EPR spectrometers at frequencies below X-band have been reviewed comprehensively (*1*). In the following paragraphs, we cite selected publications relevant to the work reported in this paper. Most prior spectrometers have been for continuous wave (CW) operation. The most complete descriptions of EPR spectrometers in the 250–300 MHz range are those of Halpern et al. (*5, 6*), Symons and others (*7–9*), and Krishna and coworkers (*10–17*). These spectrometers

Received 10 October 2001; revised 11 November 2001; accepted 12 November 2001.

Correspondence to: Gareth R. Eaton; E-mail: geaton@du.edu.

Concepts in Magnetic Resonance (Magnetic Resonance Engineering), Vol. 15(1) 59–91 (2002)

were constructed for the study of biological specimens. Pulsed EPR spectroscopy at low radiofrequency (RF) was performed at 17.4 MHz by Blume in 1958 (*18*) and more recently has been performed with nuclear magnetic resonance (NMR) spectrometers (*19–26*) and with purpose-built spectrometers in the laboratory of Krishna (*10–17*) and Sotgiu (*27, 28*).

The Halpern spectrometer used a strip-line-type resonator (~1.25 cm radius) that could hold a small mouse and a hybrid coupler to direct RF to and from the resonator (*5, 6*). It used an air-core Helmholtz magnet to generate the magnetic field and splayed these coils to create the gradient in the z direction. Gradients along the x and y directions were generated with Anderson-type gradient coils. This spectrometer is described in considerable detail, including the structural and electronic aspects of the automatic coupling control, automatic frequency control (AFC), and the strip-line resonator. The bridge design uses high dynamic range double-balanced mixers to accommodate animal-induced changes in reflected power.

The CW L-band spectrometer in the Berliner laboratory has been described (*29–32*). There have been many reports of low-frequency EPR spectroscopy from the Swartz laboratory, whose 1 GHz spectrometer was briefly described in Nilges et al. (*33*). Symons (*9*) has given a brief description of a 250 MHz spectrometer intended for whole-body human imaging. The overall design is similar to that of a smaller 300 MHz system (*7*). One of the resonators is a 45 cm diameter three-loop-two-gap loop gap resonator (LGR) (the two outer loops are 10 cm). The Q of ~300 was reduced to ~100 upon inserting a human head. The Symons 300 MHz spectrometer was designed for samples up to about 5 cm radius.

An enabling technology for low-frequency EPR is that of lumped circuit microwave resonators that permit a higher filling factor and higher B_1 per watt than cavity resonators at these frequencies (*34*). Rectangular cavity resonators or cylindrical cavity resonators would be extremely large at these low RFs [see the review by Hyde and Froncisz (*35*)]. The crossed-loop resonator (*36–39*) used for pulsed EPR in our spectrometer is described in an accompanying paper (*40*). Sotgiu and coworkers incorporated reentrant resonators and multipole magnets, which can produce magnetic field gradients in low-frequency EPR imaging systems (*41–45*).

It is not necessary to build a spectrometer if the goal is spectroscopy and imaging of small objects at L-band, since a fully functional spectrometer that takes advantage of some of the software developed for magnetic resonance imaging is available from Bruker BioSpin, EPR Division. The Elexsys E540 L-band imaging system performs two-and three-dimensional spatial imaging and spectral-spatial imaging. The resonator has 34 mm free access diameter.

The spectrometer described in this paper differs from prior spectrometers in the design of the bridge, magnet, resonator, and pulse timing system. This spectrometer has been designed for maximum flexibility for testing alternative components and will be used in the future to seek improved performance of pulsed 250 MHz EPR. In addition, the spectrometer is designed with the intent that as it evolves it will be compatible with commercial spectrometer components to facilitate transfer of technology to other laboratories.

MATERIALS AND METHODS

The 250 MHz spectrometer builds on prior EPR spectrometer design experience in our laboratory (e.g., *46–49*). The spectrometer is designed from an EPR perspective and differs from typical NMR spectrometers in spite of operating at a frequency common in NMR. Thus, for example, the bridge is built around a circulator, as is common in microwave-frequency EPR spectrometers. Although there are many ways to detect electron paramagnetic resonance, we have chosen to restrict the design of the spectrometer described here to two fundamental types of measurements: CW detection with magnetic field modulation and phase-sensitive detection at the modulation frequency and electron spin echo (ESE) detection. These choices were based on the general experience that these methods yield the best signal-to-noise ratio (S/N) and with a view toward applications that include CW and pulsed EPR in vivo imaging, electron spin relaxation time measurements, and electron spin echo envelope modulation for determination of nuclear-electron interactions in proteins. The choice of 250 MHz is based on the considerations of depth of penetration into animals outlined by Halpern and Bowman (*6*).

A circulator efficiently routes the source power to the resonator and the EPR signal from the resonator to the detector. Either, but not both, of these paths can be made low-loss with a directional coupler. The primary disadvantages of using ferrite circulators and isolators in a very high frequency (VHF, 30–300 MHz) bridge are that they are narrow band and are sensitive to changes in the magnetic field. Although octave bandwidth circulators and isolators are available above 1 GHz, in the VHF region, bandwidths commonly are ~10%. This requires that the operating frequency be chosen early in the design and hence requires that the resonator be designed to work within the bandwidth

of the circulator. Isolators, which in general are used to absorb the power from a mismatched load and which help reduce the impact of switching transients on other active devices, are circulators with one port terminated in a matched load. Consequently, isolators have the same bandwidth limitations as do circulators. Greater flexibility in choice of frequency is desirable and is an advantage in the design of some prior spectrometers.

There is a general tradeoff between bandwidth and other performance features of many components used in the bridge. We selected components for optimum performance near 250 MHz. Of the components listed in Table 1, a large fraction have bandwidths narrow enough to prevent increasing or decreasing the operating frequency by as much as a factor of 2.

A dominant feature of the design philosophy for this spectrometer was maximum flexibility to test alternative approaches to both CW and pulsed EPR and to test various magnets, power supplies, RF sources, RF amplifiers, resonators, etc. This requirement resulted in considerable complexity that was only slightly decreased by modular construction. It became evident that the incident RF and EPR signal paths had to be switched in so many combinations that the losses would be unacceptable. Consequently, we adopted as a central design feature the use of small plug-in circuit cards containing microstrip circuits that redirect the circuit paths for each of the four combinations of LGR, crossed-loop resonator (CLR), CW, and pulse. The circuit cards can be changed quickly and this can be done with power on if the bridge is in "standby" mode.

Most components in the bridge are connectorized for ease of replacement or interchange and have SMA connectors. Most RF excitation and signal paths inside the bridge use 0.141 inch flexible coaxial cable or semirigid coaxial cable. Outside the bridge, RG-58/U coaxial cable with BNC connectors is used for most signal paths. Paths from the RF source to the bridge, from the bridge to the resonator, and, in the case of the CLR, from the resonator to the detection system, use ⅜-inch diameter coaxial cable type RG-8U with BNC-type connectors, which has much lower loss than does RG-58U cable.

General

The VHF (~250 MHz) EPR spectrometer designed and built by the University of Denver (DU) consists of a number of subsystems and operates in a number of different modes. Each of these subsystems will be described. The operational modes optionally use either the DU-designed data acquisition and control system or the Bruker E540 console or a combination of both. There is a choice of two different magnets, an 81 cm air-core magnet described separately in this issue and a 40 cm air-core magnet. As described there, the magnet was designed to have good homogeneity over a large volume of sample and to provide ease of access to the sample from either the direction parallel with or perpendicular to the magnetic field. In addition, the 81 cm air-core magnet was constructed with a nonmetallic support to minimize eddy currents during rapid scans of the magnetic field. Either the Bruker or DU system can control the 81 cm magnet while to date only the DU system controls the 40 cm magnet.

The choice of EPR signal detection scheme is also fundamental to the design of a spectrometer. Traditionally, CW EPR spectrometers operating in the 1–35 GHz range have used crystal detectors to rectify the microwave signal from the resonator. High-frequency spectrometers commonly use bolometers. Pulsed EPR spectrometers, especially those designed for ESE or free induction decay (FID) detection, have used a double-balanced mixer (DBM) or quadrature mixer. We have used DBM detection and quadrature mixer detection in our locally built spectrometers because the DBM retains phase information. As described in Refs. *46* and *47*, switching the phase of the Local Oscillator (LO) side of the DBM rapidly during pulse sequences makes it possible to perform rapid subtraction of signals in phase-cycled pulse sequences. A DBM also helps decrease sensitivity to phase noise from the source. The quadrature mixer provides phase-quadrature signals that can be combined in computer postprocessing, so that it is not essential to set the phase exactly prior to data acquisition. For some other functions of the spectrometer, it is more convenient to use a crystal detector, as described below for AFC and for finding the resonant frequency for an overcoupled resonator in pulse mode. These considerations led to different types of detectors at specific locations in the bridge.

One can envision that as analog-to-digital converters with requisite speed and resolution become available and computer speed increases for postprocessing of EPR signals, it may be advantageous to fully digitize CW and time-domain signals at the 250 MHz RF. For example, in a recent paper from the Hyde laboratory, analog-to-digital conversion of an intermediate frequency signal was performed at 187.5 MHz in an X-band pulsed spectrometer (*50*). With available technology, we use mixers or crystals to convert 250 MHz RF to lower frequencies (rapidly changing "direct current"), and then digitize the FID

Table 1 Components for Optimum Performance Near 250 MHz[a]

(1) Fluke signal generator model 6080A
(2), (13), (20), (69) 20 dB directional coupler, Merrimac CRM-20-500
(3), (4) 1-69 dB step attenuator, Weinschel 3010-100
(5) Amplifier, 1 W, NF = 8 dB typ, gain = 13 dB min, 15 dB typ, Miteq AMP-1389-7880
(6) Circulator, 256 ± 5 MHz, UTE CT-1503-0
(7), (10) 3 pole switch, Dow Key 435-5208
(8) Low-noise amplifier, 28.4 dB gain, NF = 1.2 dB, Miteq AM-2A-000110
(9) Low-noise amplifier, gain = 15.5 dB, NF = 2.5 dB, Miteq AU-1A-0150
(11) Low-pass filter, 450 MHz, Mini-Circuits SLP-450
(12) 10 dB directional coupler, Merrimac CRM-10-500
(14) DBM, Merrimac DMM-2-250
(15) Mechanical phase shifter, Sage 6709
(17) 90, 180 phase shifter, Vectronics DP620.225-67HS
(18) DC block, Inmet 8039
(19), (42), (43), (63), (73), (77), (84), (86), (87), (88), (99), (100) Coaxial switch, 12 V, Dow Key 401-2208
(21) 100 kHz amplifier, DU 16817A
(22), (31) Detector diode, zero bias Schottky, Omniyig ODZ0501AR
(23) Not used
(24) 70 kHz AFC preamp, DU 16817C
(25) 70 kHz oscillator, DU built from International Crystal TO-11-70 kHz
(26) AFC and Smith Chart circuit card, DU 17024
(27) 90° hybrid splitter, Merrimac QHM-6-165
(28), (29), (90), (91) DBM, Mini-Circuits ZFM-3
(30), (82), (89) 3 dB, 0° splitter, Mini-Circuits ZFSC-2-1
(32) AFC amplifier, 12.5 dB gain, NF = 2.3 dB, Cougar AC540C
(33), (34) Transfer switch, Dow Key 411C-2208
(36) AFC deviation meter, R&R Instruments 288-112-EMEM
(37) Not used
(39) Panel meter, ±200 mV, $3\frac{1}{2}$ digit LCD, Acculex DP-650
(40) High-pass filter, Mini-Circuits SHP-150
(41) Frequency counter prescaler, DU 16878
(47), (48), (95) 50 Ω load, SMA
(49) High-power directional coupler, 30 dB, Werlatone C6137
(51), (78), (81) Directional coupler, 15 dB, Mini-Circuits ZEDC-15-2B
(52) Amplifier, 38.5 dB gain, NF = 2.3 dB, max output +30 dBm, Miteq AUP-1479
(53) Step attenuator, 0–60 dB, 10 dB steps, Weinschel 116A-60-66
(54) Variable attenuator, 0–20 dB continuous, Weinschel 910-20-11
(55) Power amplifier, 400 W peak, 56 dB gain, TTL blanking, CPC 8T400
(56) High-power directional coupler, 50 dB, Werlatone C6117
(57) Isolator, Channel Microwave AU369, 225–275 MHz
(62), (93) Video amplifier, selectable gain, DC coupled, DC offset, DU 17023A
(64) Quadraphase phase shifter, Pulsar model MO-B2-412
(65) GaAs switch, absorptive, SPDT, Mini-Circuits p/n ZASWA-2-50DR
(66), (71) High-pass filter, Mini-Circuits SHP-100
(67) Crossed diode noise blanking circuit, DU 17012
(68) Detector diode, Alan Industries 50D-1
(70), (97) GaAs switch, absorptive, Mini-Circuits ZYSWA-2-50DR
(72) Adjustable attenuator, Alan Industries 50CAL10, 0–10 dB
(74) Directional coupler, cryogenic, nonmagnetic, 20 dB
(75) Low-noise preamplifier, cryogenic, Berkshire Technologies U-250-2
(76) Passive limiter for detector protection, begins to limit at +6 dBm, DU 17013
(79), (80) Det. diode, zero bias, Advanced Control Components ACTP-1629PC3
(83) Isolator, Channel Microwave AU 369, 225–275 MHz
(85), (94) Scope switching circuit, DU 17025
(92) Hybrid 90° splitter, Synergy Microwave DQK-705S
(96) Fixed attenuator, 6 dB
(97) X10 amplifier, DU 17035
(98) Passive limiter with sensing circuit, DU 17013A
(101) 10 dB attenuator
(102) Amplifier, 19 dB gain, NF = 3.8 dB, Mini-Circuits ZFL-500HLNB
(103) Directional coupler, 10 dB, Mini-Circuits ZFDC-10-1

[a] Component numbers ( ) correspond to reference numbers in Figs. 5 through 8 and Fig. 13. NF, noise figure.

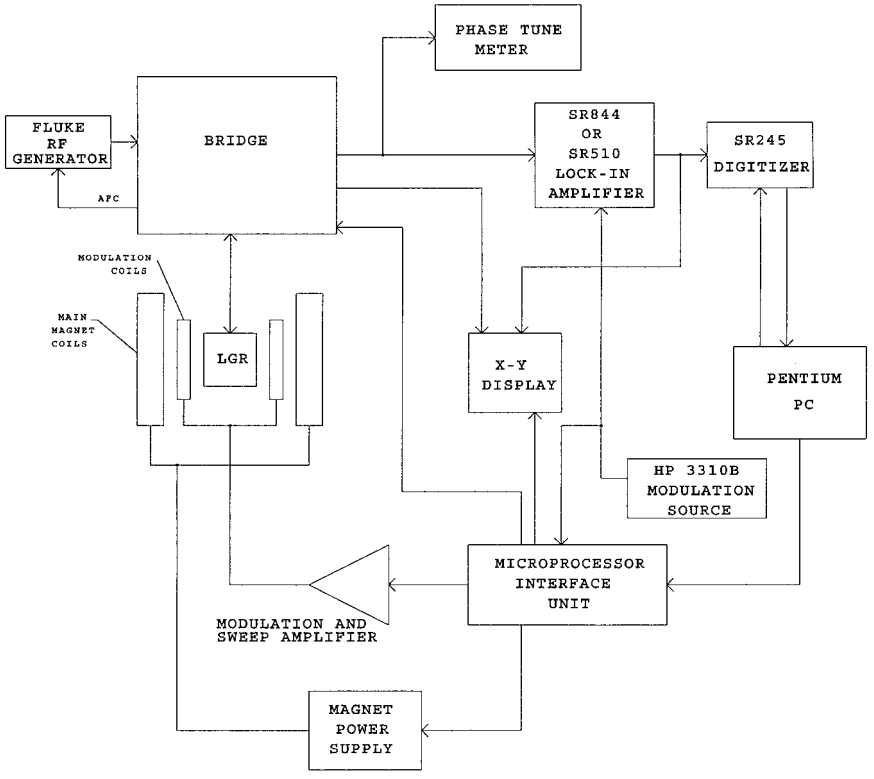

Figure 1 Block diagram of DU CW mode.

in a Bruker SpecJet or sample an echo signal with a boxcar averager.

In the spectrometer described in this paper, the EPR signal is generated in a resonator, and after transformation and coupling to the transmission line as described in detail in previous papers from our laboratory (*48, 51, 52*), the S/N is degraded by all losses and by the noise figures of all active devices (e.g., amplifiers) in the signal path. In addition, source noise reflected from a reflection resonator combines with the signal to reduce the S/N below that inherent in the thermal noise of the resonator and sample. Consequently, the selection of a CLR is a fundamental design philosophy. The CLR isolates the EPR signal from source noise and decreases the dead time in pulsed EPR, as described in Ref. *40*. The isolation provided by the CLR also permits placing the low-noise signal amplifier close to the output of the resonator, which cannot be done with a reflection resonator.

Many of the modules of this system were designed and constructed locally, that is, in the laboratories of the University of Denver. A complete documentation package including all engineering figures and schematics plus additional detailed drawings not included in this paper is available from the authors.

Major Operational Modes

Various combinations of the subsystems are possible, which could result in many different operational modes. The four major operational modes that will be described here are:

1. DU CW
2. Bruker CW
3. DU pulse
4. Bruker pulse

DU CW mode. Figure 1 shows the system components used in mode 1, the DU CW mode. In this mode the resonator is most commonly a reflection resonator (LGR) but a CLR (*36–40*) can also be used. The magnet used can be either the 81 cm or the 40 cm air-core magnet. If the 81 cm magnet is used it is powered by the Kepco power supply and if the 40 cm magnet is used it is powered by an HP model 6010A power supply. Either supply can be controlled by personal computer (PC) software via the microprocessor interface box. A complete description of the larger magnet and a brief description of the smaller magnet appear elsewhere in this issue. Each of the major subsystems is described below. In this mode the spec-

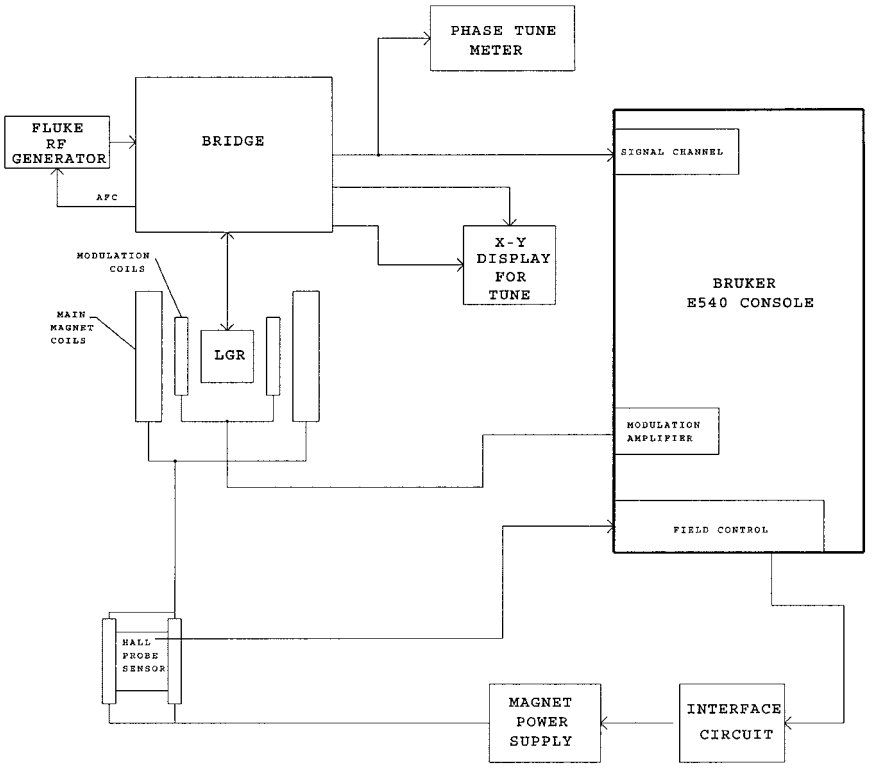

Figure 2 Block diagram of Bruker CW mode.

trometer is normally operated as a conventional CW EPR spectrometer with field modulation. The modulation coils are also used to provide a low frequency (~10 Hz) linear field sweep for the purpose of providing an oscilloscope spectral display. The field modulation and magnet are controlled from a PC using locally written software. The modulation system, the 10 Hz sweep system, the control of the magnet power supplies, and various tuning and display functions are performed by a locally designed and constructed microprocessor-controlled interface unit (described below). The field modulation frequency is supplied from an HP model 3310B function generator. Most of the bridge functions are controlled manually from the bridge front panel. The PC also controls the data acquisition and performs the postacquisition data workup. Spectral information is demodulated at the field modulation frequency by a lock-in amplifier and digitized by a locally built box that utilizes the Stanford Research model SR245 13 bit digitizer. The field modulation system utilizes a resonant drive to the modulation coils with a switch selection of two different modulation frequencies available (19 and 45 kHz). The modulation amplifier and linear sweep amplifiers that drive the modulation coils are described below. The lock-in amplifier used at 19 kHz is the Stanford Research model SR510. A Stanford Research model SR844 is used at 45 kHz. Commercial lock-in amplifiers were used because they have the needed functionality and are cost-effective relative to building these functions into the bridge. Although 100 kHz magnetic field modulation is commonly used in commercial EPR spectrometers, a current focus on narrow-line spectra makes it necessary to chose lower modulation frequencies whose sidebands are within the linewidths of the experimental spectra.

Bruker CW mode. Figure 2 shows the system components used in mode 2, the Bruker CW mode. In this mode the Bruker E540 console is used to control the field, supply the field modulation, and do the data acquisition. In this mode no low-frequency oscilloscope spectral display is available. The E540 controls the 81 cm magnet and magnet power supply (Kepco model ATE 36–30M) through an interface circuit locally designed and built, described separately below, and the Hall sensor described elsewhere in this issue. Control of the 40 cm magnet with the E540 has not yet been implemented. The Bruker system also supplies the lock-in function through its normal signal channel. The DU bridge and resonator configurations

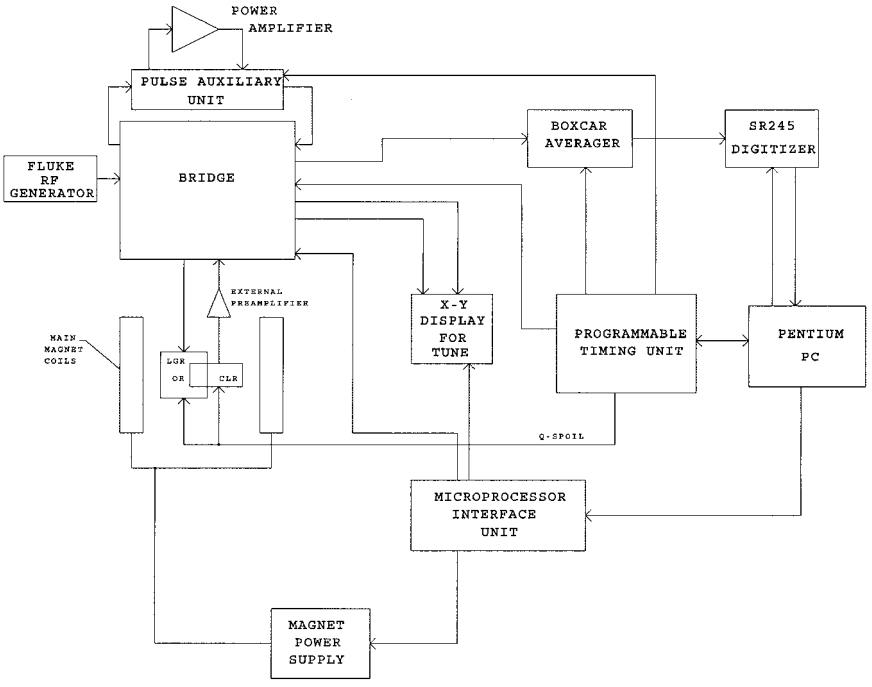

Figure 3 Block diagram of DU pulse mode.

available are the same as in mode 1. The modulation coil driver system in the Bruker console was designed for much smaller, lower inductance modulation coils than we use here [the 7 inch (17.8 cm) coils described below]. Therefore only modest modulation amplitudes are possible even when the nominal modulation amplitude is set to very high values. There are resonator capacitor selections that approximately resonate the 7 inch coils up to about 50 kHz and down to about 15 kHz, but at some frequencies the Bruker capacitor selections are too widely spaced to obtain perfect resonance. We also found that we could run the modulation system unresonated and obtain useful modulation amplitudes in the 1–10 kHz range. As noted in the prior section, these low modulation frequencies are needed for very narrow-line spectra, such as the trityl radicals (*53*). For a specific modulation field goal, coils could be designed to match the Bruker system.

DU pulse mode. Figure 3 shows the system components configured for mode 3, the DU pulse mode. In this mode the field can be controlled from the PC, using locally written software. Optionally the field can be controlled by the Bruker console if the 81 cm magnet is in use. The bridge can be configured for either a reflection resonator or the CLR. Best results are generally obtained using the CLR due to the isolation between the source and the detected signal. In addition, the *Q*-spoiling circuits used with the CLR substantially reduce the measurement dead time, as described in another article in this issue (*40*). In this mode the locally designed programmable timing unit (PTU) (*54–56*) controlled by the PC provides all of the timing functions necessary to do the various standard two- and three-pulse ESE experiments as well as more advanced experiments involving complex pulse sequences. Data are collected into a locally designed boxcar averager and digitized by a locally constructed digitizing box utilizing the Stanford Research model SR245 digitizer.

Bruker pulse mode. Figure 4 shows the system configuration for mode 4, the Bruker pulse mode. In this mode the E540 console is used to control the field, and data are digitized using the Bruker SpecJet. In this mode the PTU provides all of the timing control including a trigger to the SpecJet. Because this is the only timing interface between the PTU and the Bruker console, this mode is limited to FID experiments and fixed-pulse sequence ESE. Eventually we plan to control the timing aspects of the experiment from the PatternJet unit in the Bruker console, and this will permit collection of stepped-pulse ESE data into the Bruker. As in the DU pulse mode, the bridge can be configured for either an LGR or CLR resonator.

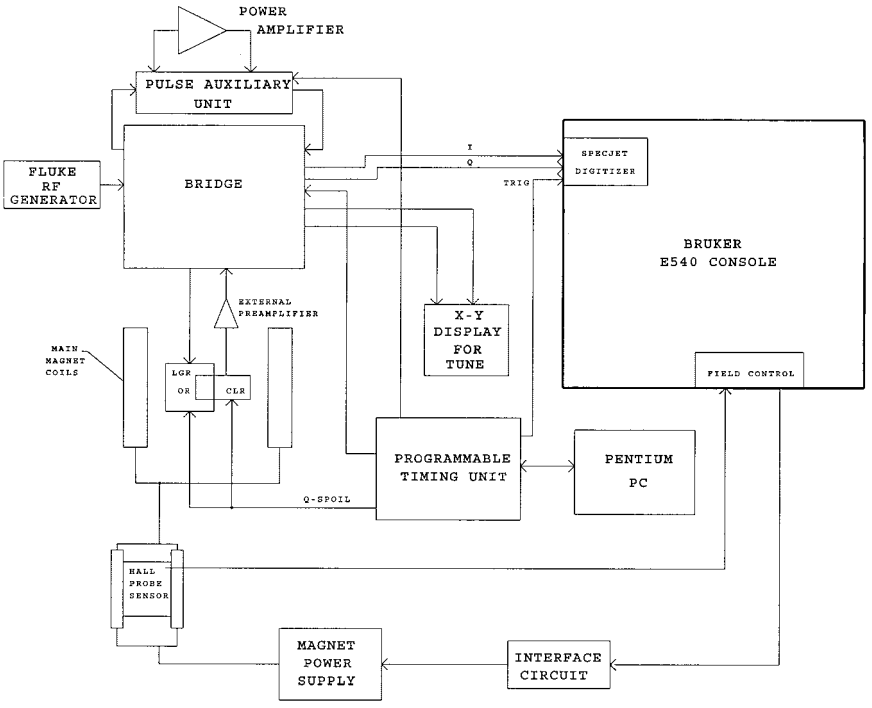

Figure 4 Block diagram of Bruker pulse mode.

Detailed Description of Spectrometer Components

Bridge

General. The overall block diagram of the pulse and CW bridge is shown in Figs. 5 through 8. Part numbers and manufacturers for the circled reference numbers are detailed in Table 1. The operational modes of the bridge are detailed in Table 2. A detailed bridge wiring schematic diagram is available. The bridge is constructed with all connectors, power supplies, and control interfaces such that it can be plugged directly

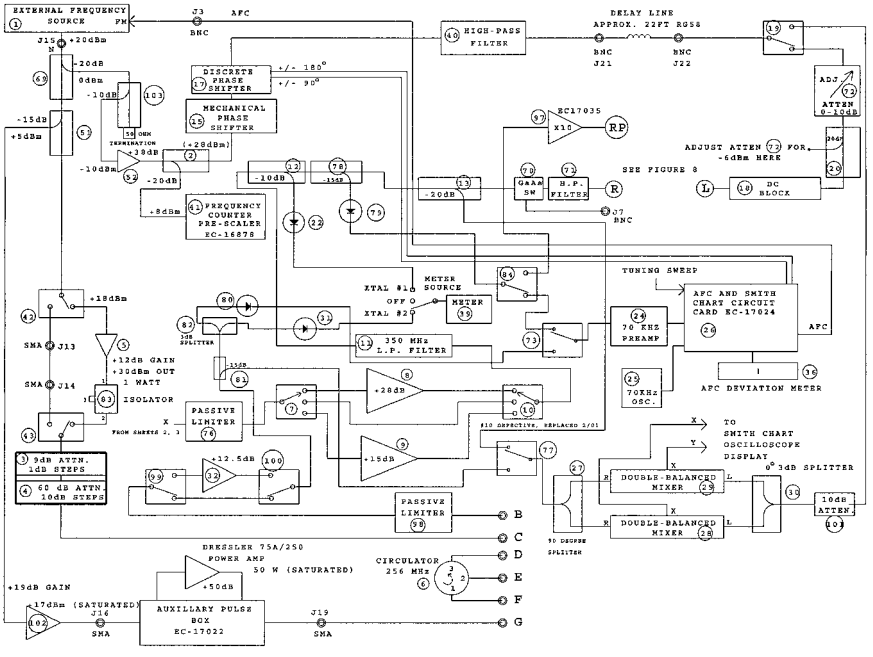

Figures 5 through 8 Block diagram of DU-constructed VHF bridge.

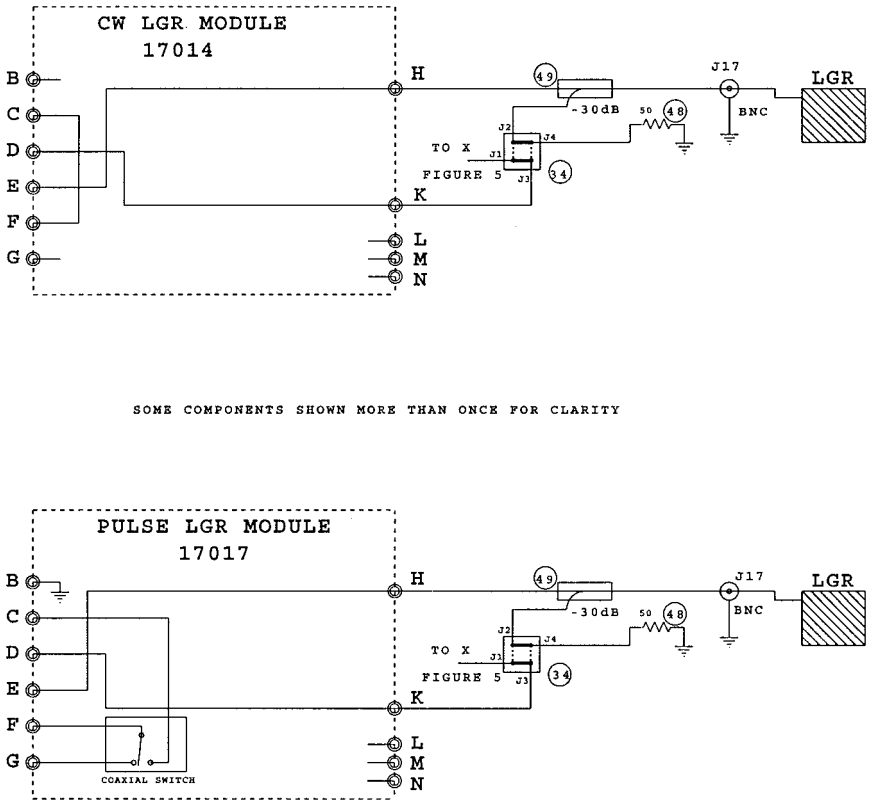

Figure 6

into a Varian E-Line console in place of the Varian bridge. The bridge is not equipped with motorized remote control features that are compatible with a Bruker bridge controller. The description given here is the operation of the bridge when connected to locally designed and constructed console functions and controls.

Front Panel Controls. Figure 9 is a representation of the bridge front panel. These are the manual bridge controls that are not computer controlled. The front panel of the bridge is 44.8 cm × 31.1 cm and is silk-screened black on a white background. The choice of manual controls was a fundamental design specification, since flexibility and versatility were a high priority, and it was desired to be able to change hardware features without having to also change software.

RF Source. Most RF sources exhibit phase noise that will dominate the noise of an EPR spectrometer at most practical power levels. The shape of the phase noise vs. frequency plot differs depending on the way the source was built. One source or another may be preferable, depending on the modulation frequency to be used. The better the source, the higher the power you can operate without S/N being limited by source noise. The lower the Q of the resonator is, the higher the power at which the source noise begins to dominate.

The RF source is a Fluke signal generator model 6080A. We also used an HP model 8640B as a source but found that because it was not digitally synthesized the frequency was too unstable for this application. The Fluke is stable but does not have the very best phase noise specifications that are available in the latest signal generators. In our applications to date, this compromise in phase noise performance has been acceptable, because the primary focus has been on time-domain spectroscopy and on use of the CLR. Generally phase noise is a less serious problem with a CLR than with a LGR. One advantage of the CLR is that it isolates the EPR signal from the source noise by the amount of the isolation between the loops, which can be at least 40–50 dB. In one test at 250 MHz, the noise was essentially constant with incident power when a CLR was used, but increased sharply with increasing power with an otherwise similar LGR. Future experiments may require a RF source with lower phase noise.

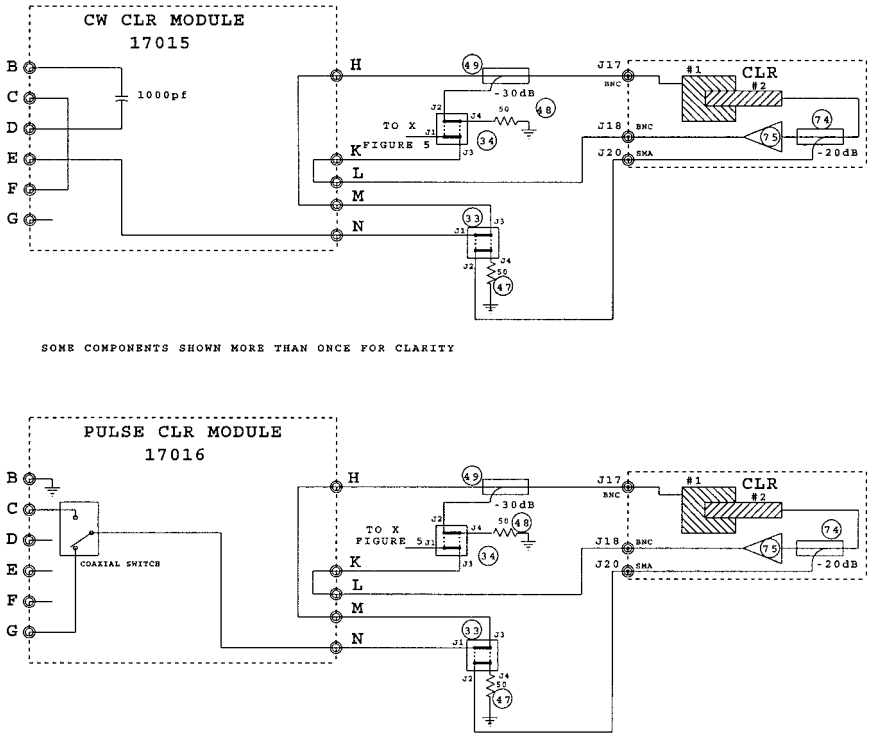

Figure 7

CW Power Distribution. CW power distribution in the bridge is shown in Fig. 5. The CW source is a Fluke generator, external to the bridge, supplying a +20 dBm power level. The forward path to the resonator is amplified by amplifier 5, to the +30 dBm (1 W) level. After losses in switching elements, cables, and connectors, approximately 850 mW is available at the resonator. A low-power path is also available that bypasses the 1 W amplifier which supplies ~50 mW at the resonator. This path is useful for experiments in which it is desired to have the lowest noise source power available and which do not require more than

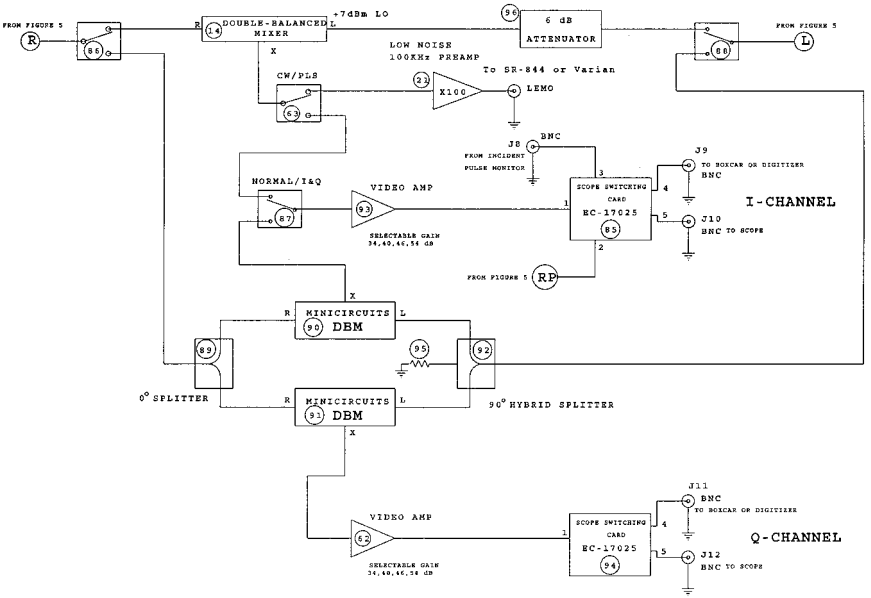

Figure 8

Table 2 Operational Modes of the Bridge[a]

Mode	Plug-In Module	Tune/Operate Switch	Resonator Mode Switch	Smith Chart On/Off Switch	$x - y$ Scope Display	Pulse Scope Display	AFC Operation
1	CW LGR	Tune	LGR	On	SC or Dots-Circ	Off	Off
2	CW LGR	Tune	LGR	Off	XTAL dip	Off	Off
3	CW LGR	Operate	LGR	Off	EPR	Off	Locked to LGR
4	CW CLR	Tune	Tune #1	On	SC or Dots-Circ	Off	Off
5	CW CLR	Tune	Tune #2	On	SC or Dots-dir. coupler	Off	Off
6	CW CLR	Tune	CLR operate	On	Isolation circles	Off	Off
7	CW CLR	Operate	CLR operate	Off	EPR	Off	Locked to #1
8	Pulse LGR	Tune	LGR	On	SC or Dots-Circ	Off	Off
9	Pulse LGR	Tune	LGR	Off	XTAL dip	Off	Off
10	Pulse LGR	Operate	LGR	Off	Off	I, R, or TD EPR	Off
11	Pulse CLR	Tune	Tune #1	On	SC or Dots-dir. coupler	Off	Off
12	Pulse CLR	Tune	Tune #2	On	SC or Dots-dir. coupler	Off	Off
13	Pulse CLR	Tune	CLR operate	On	Isolation circles	Off	Off
14	Pulse CLR	Operate	Tune #1	Off	Off	Reflected Pulse	Off
15	Pulse CLR	Operate	CLR Operate	Off	Off	Incident Pulse or TD EPR	Off

[a] Abbreviations: SC, Smith Chart; Dots, fixed, not swept, frequency display; Circ, via circulator; dir. coupler, via directional coupler; TD, time domain.

50 mW incident power. In both cases the power at the resonator is adjustable over a 70 dB range in 1 dB steps using the attenuator 3,4 front panel control. The reference arm of the bridge is used for both CW and pulse operation. Amplifier 52 provides sufficient power to drive a long delay line in the reference arm. The delay line is ~22 ft of RG/58U coaxial cable that is external to the bridge box. The delay line is neces-

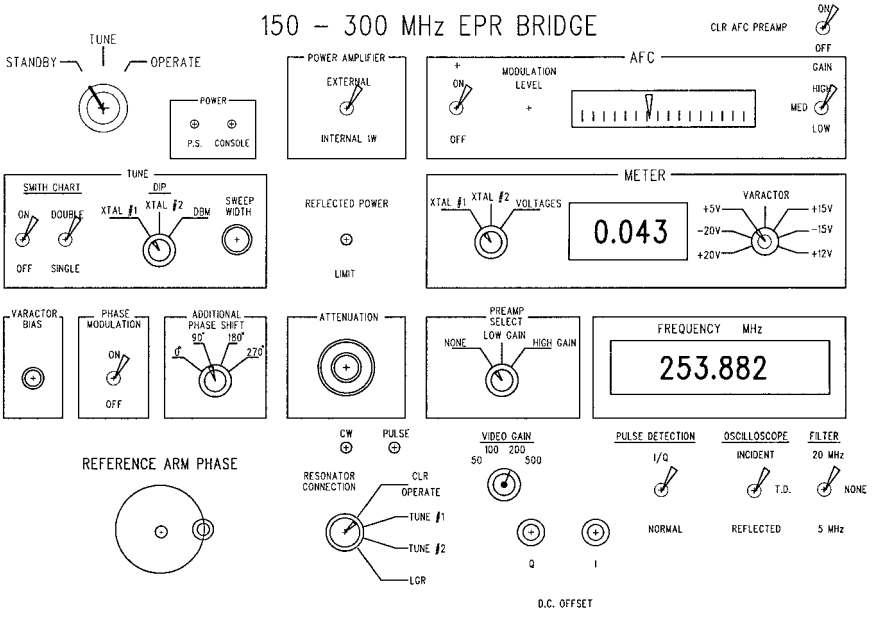

Figure 9 Front panel of DU-constructed VHF bridge.

sary to approximately match the phase delay of the reference arm to that of the path to the resonator and back. By matching these delays the detection mixers provide better phase noise rejection by keeping the noise in the reference path coherent with that in the signal path. This is equivalent to saying that all frequencies have equal delays or what is known as flat group delay response in communication systems. The reference arm phase is front panel adjustable by mechanical phase adjuster 15 and discrete phase shifter 17. At this frequency the mechanical phase adjuster can only shift the phase a little more than 90° end to end. The discrete phase shifter has four 90° steps so that a total of a bit over 360° of phase shift adjustment is possible. The discrete phase shifter is also used in the Smith Chart tuning mode to chop the display (see description under "Resonator Tuning System," below). Directional coupler 103 (10 dB) is used in addition to coupler 69 (20 dB), because an appropriate 30 dB coupler was not available at 250 MHz.

Frequency Counter. The front panel of the bridge displays the source frequency to six digits of resolution and accuracy. The time base standard for this display is a temperature compensated crystal oscillator (356BC, Oak Technology, Sunnyvale, CA). The frequency counter was designed and built locally. It consists of a prescaler circuit, item 41 in Fig. 5, and a counter card and a display card. Detailed schematic diagrams of the prescaler, counter, and display cards are available. The prescaler divides the source RF by a factor of 256 and provides a transistor-transistor logic (TTL) level signal to the counter card. The prescaler also divides the input frequency by 1024 for use in the Bruker frequency counter. The counter in the bridge is a gated counter design providing an updated display every 512 ms. The measurement gate is 256 ms long. The large format LED display elements visible on the front panel of the bridge are mounted on the display card. Using other prescaler circuits we have adapted this counter circuit to other spectrometers in our laboratory, including X-band. We have also supplied this counter as a stand-alone unit to other laboratories.

Resonator Tuning System. Resonator tuning is critical for spectrometer performance. This is especially true in the case of the CLR in which the frequencies of two resonators must be matched. In pulse mode where overcoupling may be desired it is important that the degree of overcoupling and the Q be known. It is also important that any tuning mechanism used be such that the resonator and its coupling mechanism stay in the tuned condition when the system is switched from TUNE to OPERATE. It is anticipated that a wide variety of resonators, including reflection and crossed-loop resonators will be tested with this spectrometer. Experience with one CLR is described in an accompanying paper. For these reasons we have built into the bridge an extensive set of resonator tuning facilities.

Smith Chart Display

The bridge incorporates a Smith Chart coupling display, which we have found to be generally more useful and easier to interpret than the customary "dip" in the display of the reflected power vs. frequency (*57*). The reflected signal is obtained through circulator 6 (Fig. 5) in modes in which the circulator is required in OPERATE (i.e., all LGR modes and the CLR CW mode). In modes in which the circulator is not used in operation (i.e., pulse CLR modes), directional couplers 49 and 74 (Figs. 6 and 7) are used to obtain reflected signals for resonator tuning. Transfer switches 33 and 34 switch to the appropriate signal paths for tuning the various resonator configurations. When the Smith Chart display is in use, coaxial switch 19 redirects the reference arm power to Smith Chart mixers 28 and 29. These mixers operate in quadrature from 90° hybrid coupler 27 and in-phase power divider 30. The intermediate frequency (IF) port of each of these mixers is directed to amplifiers in the microprocessor interface box (see details below) and ultimately to the *x-y* display oscilloscope. The Smith Chart can optionally be operated in the conventional single trace mode or in a biphase chopped mode. The chopped mode is useful because it eliminates the need for a calibrated graticle on the display. In the chopped mode there are two traces 180° apart. Critical coupling is indicated when the two traces are tangent. Overlapping traces indicate overcoupling and underlapping traces indicate undercoupling. The chopping signal is developed by an oscillator on circuit card 26. The chopper frequency is adjusted to approximately 5 kHz. The exact frequency is chosen so that the beats between the chopper frequency and the frequency modulation (FM) sweep produce a smooth display. The chopper frequency is logically combined into the path of the 180° bit of the discrete phase and sent out to the phase shifter by a 50Ω driver.

Resonator *Q* Dip Displays

Although we normally depend on the Smith Chart for resonator tuning we occasionally find that a traditional resonator dip display is useful. The bridge produces a

dip display detected by crystal 79 (LGR) or crystal 80 (CLR) (Fig. 5). This detected signal is amplified by the same amplifier 24 used for the AFC preamplifier and routed through circuit card 26 where it is amplified further and provided with direct current (DC) offset control. From here it is routed to the microprocessor control box where it is ultimately sent to the *y* axis of the *x-y* oscilloscope display. Similarly, a dip display can be observed from DBM 14 (Fig. 8). In TUNE the output of this mixer is amplified by amplifier 21 and routed to circuit card 26 where it is amplified further and provided with DC offset. From here it is routed to the microprocessor control box where it is ultimately sent to the *y* axis of the *x-y* oscilloscope display. We have found this dip display from the DBM useful in adjusting the length of the reference arm delay line since it preserves phase information in addition to the amplitude response.

Reflected Pulse Display

When a resonator is adjusted for moderate to extreme overcoupling, the Smith Chart becomes less helpful for either selecting the proper operating frequency or for estimating the resonator *Q*. The bridge has a facility for observing the reflected response to an RF pulse, which facilitates a judgment of the proper frequency setting even for extreme overcoupling (see Fig. 7 in Ref. *51*). The reflected response also provides a means of measuring the resonator *Q* by measuring the ring-down time at the end of the pulse. The reflected signal is obtained through circulator 6 (LGR mode) or through couplers 49 and 74 (CLR mode) and detected by crystal 79 (Fig. 5). By using a crystal and not a DBM, the power reflected can be measured independent of the RF phase information. The crystal is in the power law detection region below 10–15 mV. We often digitize these signals so that we can obtain computer-assisted curve fits to the ring-down exponential to estimate *Q*. SpecJet is an eight bit digitizer with a 1 V dynamic range so a 10 mV signal is too small to be properly resolved, and some amplification is needed. Amplifier 97 provides a 20 dB (10×) amplification to bring the signal up to the 100 mV level which fits the digitizer much better. Amplifier 97 is locally designed and constructed.

Plug-in Configuration Modules. Figures 6 and 7 show plug-in configuration modules 17014 through 17017. These are small (9.4 cm × 4.6 cm) microstrip circuit cards, locally designed, that plug into the bridge. They reconfigure the resonator and circulator connections for the major operational modes of the bridge. There are four different configuration modules: CW-LGR, CW-CLR, pulse-LGR, and pulse-CLR. The modules are connectorized with SMB blind-mate connectors and can be removed and inserted with the power on so long as the bridge is in STANDBY mode. Microstrip coaxial switches on the pulse modules switch in CW power for resonator tuning purposes. The configuration modules were designed to eliminate additional switching paths that would have inserted additional losses and therefore noise into the signal paths. In addition, the use of plug-in modules provides flexibility for ease of modifying these functions or adding new functions in the future.

AFC. The AFC System consists of detector crystal 79 (LGR mode) or crystal 80 (CLR mode) followed by preamplifier 24, portions of circuit card 26, 70 kHz oscillator 25, and deviation meter 36. Reference numbers refer to Fig. 5. The AFC system uses a separate crystal detector rather than the DBM EPR detector so that AFC can be established without regard to RF phase. This is important because the AFC signal and absorption EPR are in quadrature to one another and therefore the best phase for absorption EPR is the worst phase for AFC. The preamplifier provides low-noise amplification of the detected 70 kHz signal with ~40 dB (100×) gain. This is followed by the portion of circuit card 26 shown in Fig. 10. In this diagram stages U1, U2, and U3 provide a gain selectable amplifier, the gain of which is selected on the front panel of the bridge. Three gain selections are available, which are preset by pots on the circuit card. Stage U4 is a moderate *Q* (~20) 70 kHz bandpass tuned stage followed by additional gain in stage U6A. This stage is followed by double-balanced mixer DBM1, which synchronously detects the signal. The reference side of the DBM is supplied through stage U6B that has pots to set the phase and amplitude of the reference. The output of DBM1 is then integrated by stage U5A. The output of the integrator is a DC error voltage that is low-pass filtered by R33 and C25 (low pass corner at 16 Hz). This error voltage is then combined with the 70 kHz alternating current (AC) component in stage U5C which is then filtered and buffered and sent to the DC FM port of the RF source generator. The AC component amplitude (AFC modulation amplitude) is set by a front panel control. Stage U5C (Fig. 10) also combines the tuning sweep ramp into the FM signal to sweep the frequency when in TUNE mode. The AFC source frequency is supplied from a locally constructed 70 kHz oscillator based on a 70 kHz fundamental mode crystal (OT-11-70 kHz obtained from International Crystal, Inc., Oklahoma City, OK). Stages U10C, U10D, U11C,

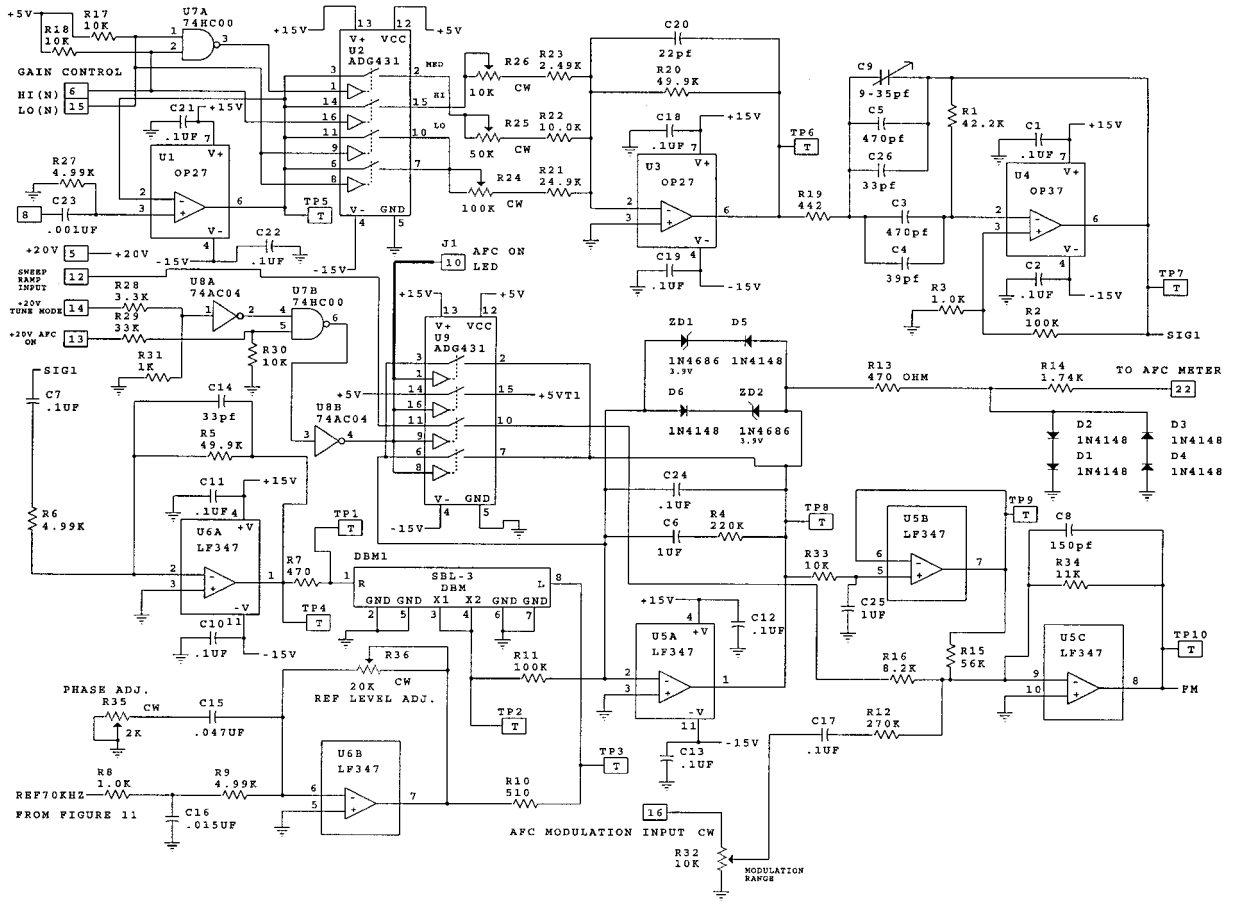

Figures 10 and 11 Schematic of circuit card 26 containing AFC and Smith Chart circuits.

and U11D (Fig. 11) provide impedance transformation, signal gain, and bandpass filtering to condition the relatively weak and distorted signal available from the crystal oscillator up to the level needed by the other circuits ($\sim$8 V_{pp} sine wave). This circuit supplies the 70 kHz reference for the detection DBM (described above) and also is sent out to the microprocessor interface to supply the reference for the phase tuning meter (described below).

Limiter. Figure 5 shows protection limiters 76 and 98. These limiters provide protection for the low noise preamplifiers. The reflection from an overcoupled resonator can be destructive to a preamplifier. The limiters are positioned to protect whichever preamplifier is selected. The limiter (Fig. 12) is made from type 1N4148 fast switching diodes. These diodes switch fast enough that at 250 MHz they perform a real-time single-cycle clipping function when the power is above $\sim$+6 dBm. With an input power of $-$20dBm the insertion loss of the limiter is not measurable. When the input power is 0 dBm the insertion loss is 0.6 dB. At +20 dBm the insertion loss is $\sim$11 dB. When the diodes are conducting the limiter becomes a mismatched load that reflects most of the incoming power back to the source where it is absorbed in isolator 57 [Fig. 13 (pulse mode)] or isolator 83 [Fig. 5 (CW mode)]. The limiter has been tested to survive and operate properly with 400 W pulses of 1 ms duration and 1% duty cycle and with 1 W of CW power. Limiter 98 also contains a DC sense circuit that detects the presence of either a pulse configuration module or a CW configuration module. The limiter is constructed on a small printed circuit card (3.81 cm $\times$ 3.75 cm) of local design and housed in a small box with SMA connectors.

External Low-Noise Preamplifier. The isolation of the CLR replaces the circulator function in a conventional EPR spectrometer designed for use with a reflection resonator (*36–40*). The CLR configuration shown in Fig. 7 allows the possibility of having the first low-noise amplifier in the signal path to be very near the resonator. This location for the low-noise RF

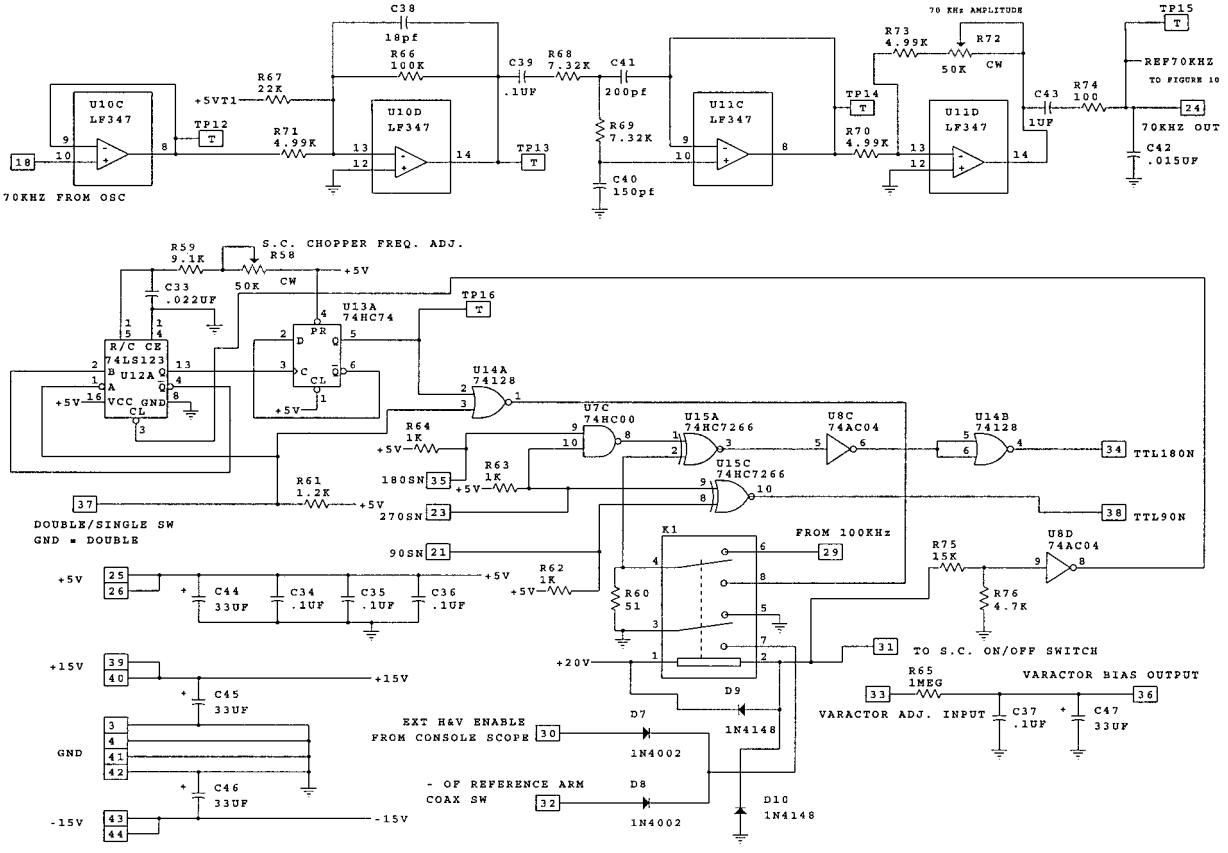

Figure 11

amplifier minimizes the signal losses prior to the amplifier, establishes the noise floor of the spectrometer, and hence yields the best S/N achievable with a given low-noise amplifier. We use a cryogenically coolable amplifier, model U-250–2 obtained from Berkshire Technologies (Oakland, CA) (item 75 in Fig. 7), to facilitate future measurements in which the resonator and the low-noise amplifier will be cooled to approximately the temperature of the sample to further improve S/N (*52*). This amplifier has ~39 dB gain at 250 MHz. To facilitate tuning of the resonator, directional coupler 74 is required between the amplifier and the resonator.

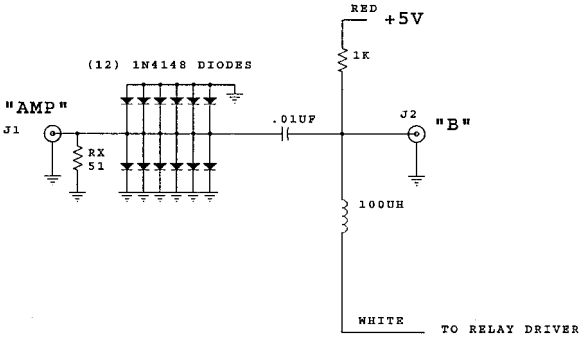

Figure 12 Schematic of protection limiter circuit.

Low-Noise Preamplifiers. Amplifiers 8 and 9 (Fig. 5), are low-noise amplifiers, Miteq AM-2A-000110 and AU-1A-0150, respectively. Low-gain amplifier 9 with +15 dB gain can often be used in addition to the Berkshire external amplifier with the CLR. This provides a total of ~54 dB of gain before the detector. In some cases the external amplifier alone gives the best results and the NONE preamplifier path is then selected on the bridge front panel. Amplifier 8 with +28 dB of gain is more often used with an LGR where no external amplifier can be used.

Detectors and Detector Blanking. In the CW mode double-balanced mixer 14 (Fig. 8) is the detector. Detector blanking switch 70 (Fig. 5) is not used in CW mode. In LGR pulse mode, blanking switch 70 is often used to blank the detector to prevent overload of the detector and video amplifiers due to the resonator ring-down. When the CLR is used with active *Q*-

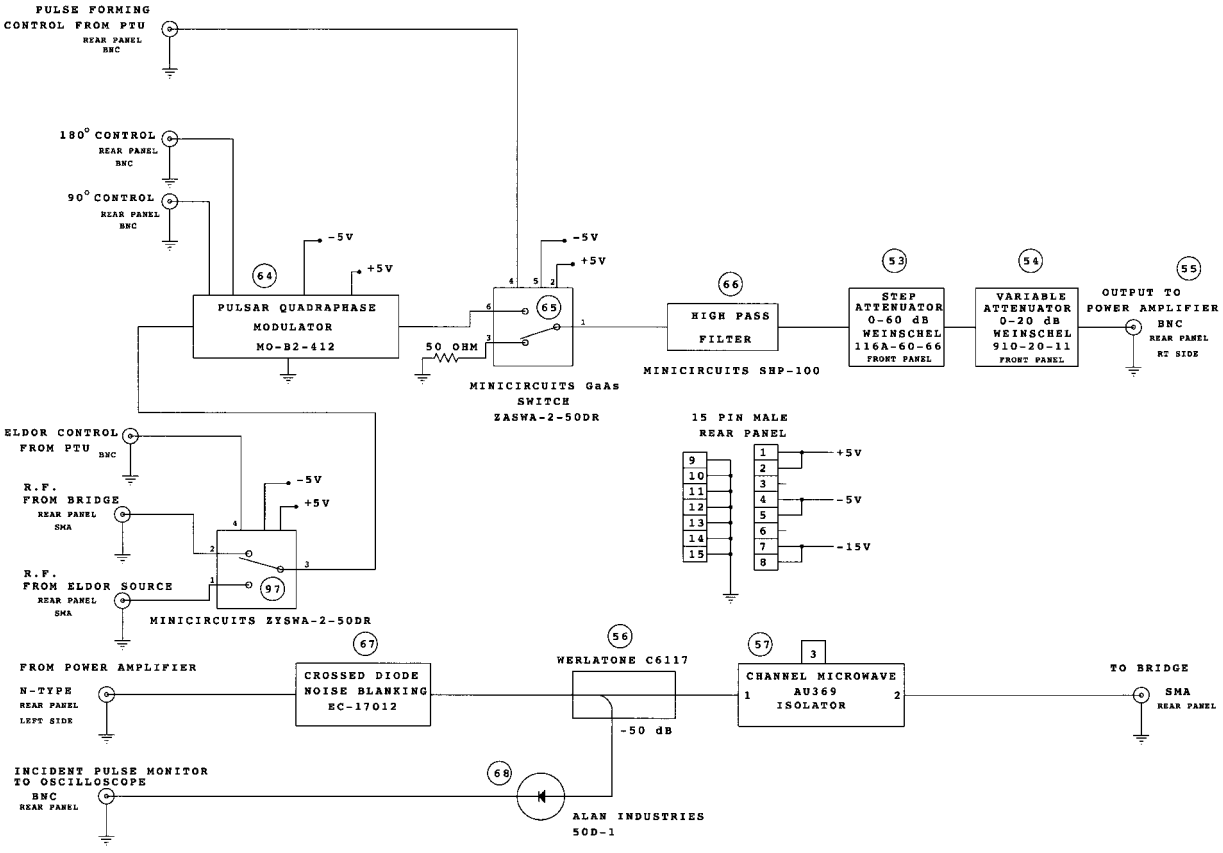

Figure 13 Block diagram of pulse auxiliary box.

spoiling we have found that the detector blanking function is not necessary. The detector blanking switch is controlled by the PTU and its time position can be set by a combination of software settings in the PC and an analog delay knob on the front panel of the PTU. In pulse mode two different detection systems are available by bridge front panel selection. In NORMAL DBM 14 is the detector, and all of the available signal is directed to this detector. Normally this single-channel detection system is used in the DU pulse mode in which data are collected in the boxcar averager. In the *I*/*Q*, or quadrature mode, power splitter 89 (Fig. 8) divides the signal between two DBMs, 90 and 91. These mixers operate in quadrature from a reference signal that is divided by 90° hybrid splitter 92. This produces detected signals *I* and *Q*, which are amplified by video amplifiers and routed to the Bruker SpecJet dual-channel digitizer (Bruker pulse mode).

CW Low-Noise Amplifier. Amplifier 21 (Fig. 8) is used to amplify the CW EPR signal before it goes to the lock-in. This amplifier is of local design and construction and is of similar design to 70 kHz AFC preamplifier 24. These amplifiers are built on small circuit cards (6.9 cm × 4.3 cm) and packaged in small shielded boxes. The low-frequency response of this amplifier has been extended below 1 kHz so that low-frequency modulation can be used. The amplifier is designed with low-noise transistors (type MPS4356) to achieve the best possible noise performance; however this amplifier will make a significant contribution to the noise floor only if no low-noise RF preamplifier is used. The nominal gain of amplifier 21 is 40 dB (100×).

Video Amplifiers. Video amplifiers 93 and 62 (Fig. 8) are used to amplify the detected signals in pulse mode before they are sent on to either the boxcar averager or the SpecJet digitizer and a monitoring oscilloscope. The amplifiers are of local design and construction. These amplifiers are gain adjustable from the bridge front panel in four steps of 34, 40, 46, and 54 dB (50, 100, 200, and 500×). They also have DC offset controls on the front panel. We have experimented with both AC and DC coupling for these amplifiers and find there are tradeoffs, and a case can be made for either coupling method. We are currently using AC coupling with the high-pass corner at 10 Hz and

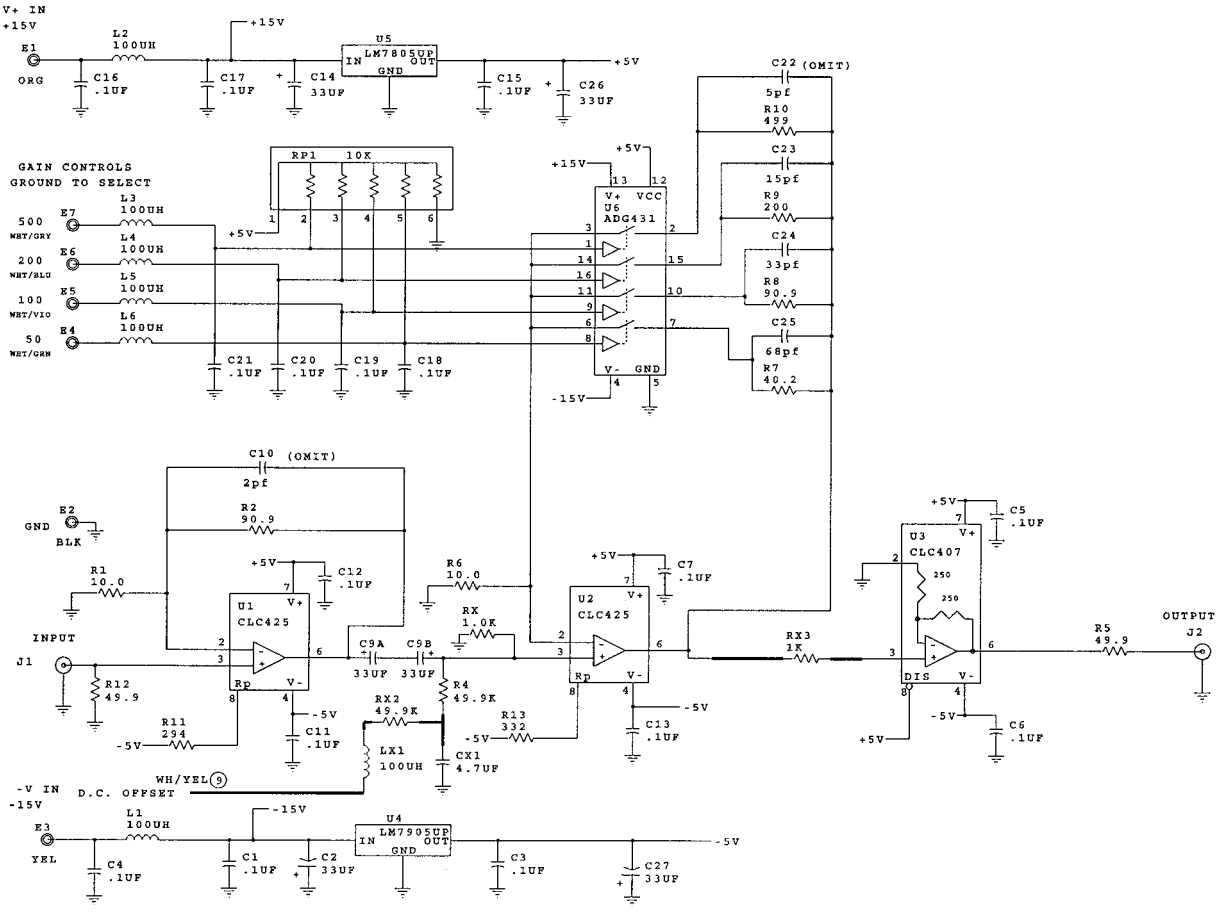

Figure 14 Schematic diagram of video amplifier.

then using the DC offset control to set the DC position of the baseline. The DC offset is injected into the circuit after the AC coupling. The amplifiers (Fig. 14) are built around the CLC425 op-amp, which to our knowledge has the lowest noise of any available consistent with the gain-bandwidth product that is required for this application. There are two gain stages followed by a cable driving stage. The bandwidth of these amplifiers ranges from 45 MHz at a gain of 50 to 8 MHz at a gain of 500. The digital control signals that bring in the gain control signals are extensively decoupled to reduce noise. Also the power supplies are reregulated on the circuit card to reduce power supply-induced noise. Integrated circuit-based amplifiers with high gain-bandwidth product are notoriously noisy. We have measured noise figures for amplifiers 62 and 93 of ~10 dB, but because of the large amount of gain in the system before these amplifiers they do not contribute materially to the overall noise floor of the spectrometer. The amplifiers are constructed on a small printed circuit card (6.86 cm × 4.32 cm) of local design and housed in small boxes with SMA connectors.

Signal Distribution and Filters. Following the video amplifiers in Fig. 8 are the scope switching cards 85 and 94. These cards (Fig. 15) provide front panel selectable filters, function selection, and signal distribution to the digitizer, boxcar averager, and monitoring oscilloscope. The front panel filter selections are 1 MHz, 5 MHz, or NONE. Signal functions that can be selected at the front panel are incident pulse monitor (derived near the output of the power amplifier from crystal detector 68 (Fig. 13), reflected pulse display (see description under the "Resonator Tuning System" above) and the time-domain EPR signal. These cards make it possible to observe the spectrometer output signals on an oscilloscope at the same time that they are also routed to either the SpecJet digitizer or to the boxcar averager. These circuits are locally designed and constructed on small printed circuit cards (10.0 cm × 5.46 cm) with SMA connectors.

Pulse Auxiliary Unit

Figure 13 shows the pulse auxiliary unit. Part numbers and manufacturers for the circled reference num-

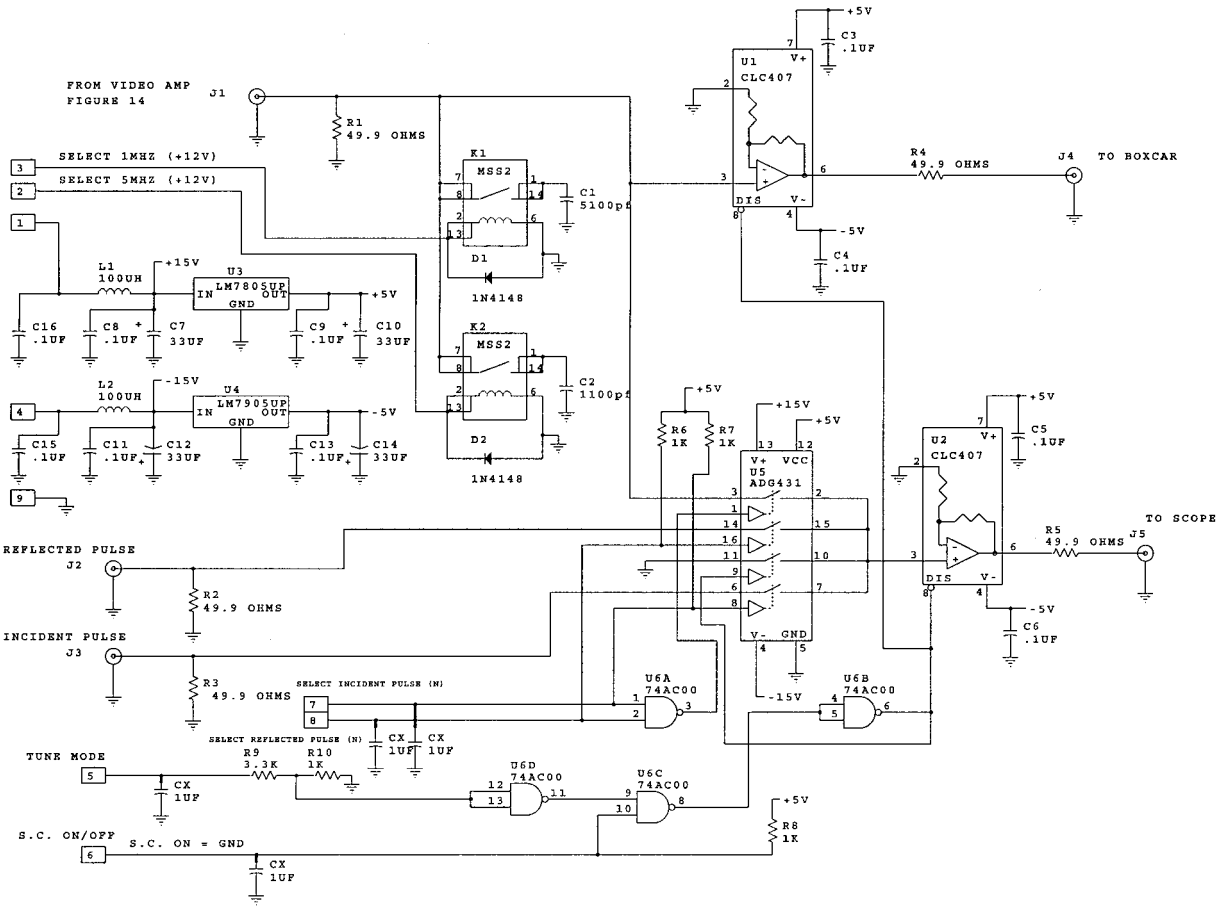

Figure 15 Schematic diagram of video distribution circuit card.

bers are detailed in Table 1. This unit contains most of the components of the power arm of the pulse system except for the power amplifier itself. Phase shifter 64 is a four-state phase shifter that allows shifting the phase of the power arm in 90° steps. Pulse-forming switch 65 forms the pulse. High-pass filter 66 attenuates video feedthrough induced by the switch. Attenuators 53 and 54 provide 0–80 dB of attenuation by a combination of step and continuously variable controls. Continuously variable attenuator 54 (Weinschel model 910-20-11) has minimal phase shift with attenuation change. Step attenuator 53 has considerable phase shift as a function of attenuation setting. By operating in a range where only the continuously variable device has to be changed, the phase can be kept reasonably constant. Switch 97 provides a path to bring in a second RF frequency for use in electron-electron double resonance experiments. In the lower portion of the figure, devices 67, 56, and 57 are in the high-power path after the external power amplifier. Coupler 56 supplies signal to monitoring crystal 68 whose output is the incident power monitor signal that is selected on the front panel to go to the oscilloscope. Crossed-diode noise blanking circuit 67 (Fig. 16) is of local design and construction. It uses small surface mount diodes (type 1N4148W) to provide a threshold of three diode levels in each direction. The noise level of the power amplifier is well below this level so the diodes are cut off until a power pulse is applied. During the power pulse the three-diode drop at the zero crossing induces a small amount of harmonic distortion, but the resonator is an effective filter that eliminates (reflects) the harmonics. The diodes have finite capacitance in the off state so the residual noise of the amplifier is not completely blanked. However, our tests indicate that this circuit pushes the noise down by ~10 dB, and we have ordered a power amplifier with internal blanking specified at 10 dB above thermal so this circuit should bring the noise essentially down to thermal level. The diagram also shows quarter-wave stub tuned short/open branches. These are designed to provide a short branch at the main line for the low-power (noise) condition and an open branch during the power pulse, thus further

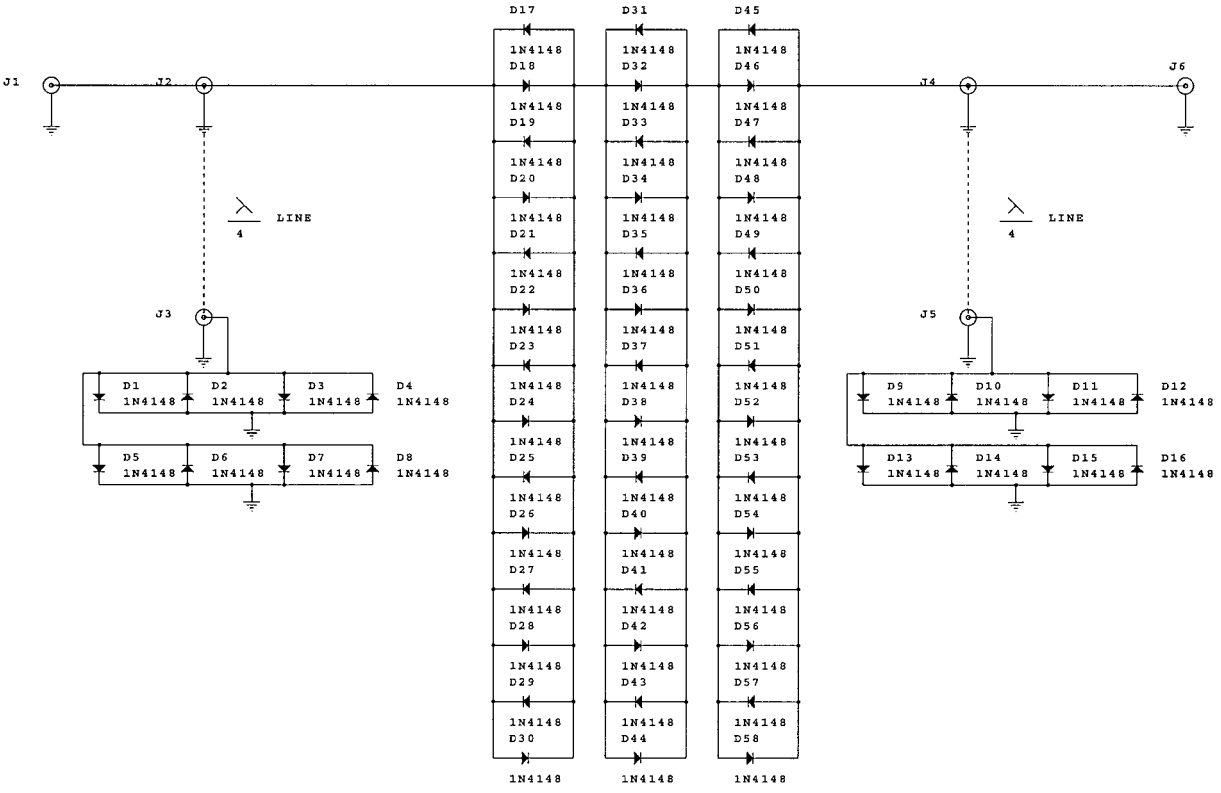

Figure 16 Schematic diagram of crossed-diode noise reduction circuit card.

eliminating noise. We have not yet tested this feature although the printed circuit card incorporates the design. The circuit card on which the noise blanking is implemented is 8.9 cm × 7.0 cm and has SMA connectors.

Power Amplifier

Pending our acquisition of an appropriate power amplifier we have done pulsed EPR measurements with a temporary amplifier, Dressler model 75A/250. It has fast rise time but no noise blanking and provides ~25 W power at 250 MHz. We plan to use a 400–500 W amplifier with noise blanking in the near future.

Microprocessor-Controlled Interface Unit

General. The microprocessor-controlled interface unit (Figs. 17 through 26) serves as an interface and control system between the PC and the major hardware elements of the spectrometer such as the bridge, modulation coils and modulation amplifier, lock-in amplifier, magnet power supplies, and oscilloscope display. The unit contains one large printed circuit card of local design (40 cm × 35 cm) on which all of the electronic components plus the input/output connectors and front panel controls are mounted. The card is arranged so that some connectors protrude through the front panel and some through the rear panel of the box

Modulation Control System. The modulation control system contains design features that permit many modes of operation. One design specification was to be able to control a calibrated current in relatively small, low inductance modulation coils over a broad band of frequencies (5–200 kHz), which could be swept to discover resonator microphonic resonances in small resonators. This required that the modulation coils not be resonated and that the modulation power amplifier be capable of driving the coils directly. This also required that the current control system operate with a current feedback element to maintain magnetic field modulation calibration at all operating frequencies. This is in contrast to fixed frequency designs such as the Varian E-line system, which is a resonated open-loop calibrated design. Later systems with more integrated computer control such as the Bruker system are able to do sophisticated computer-controlled calibration at a number of frequencies, but they still operate open-loop. For the specific large VHF resonators and large modulation coils used to date, the

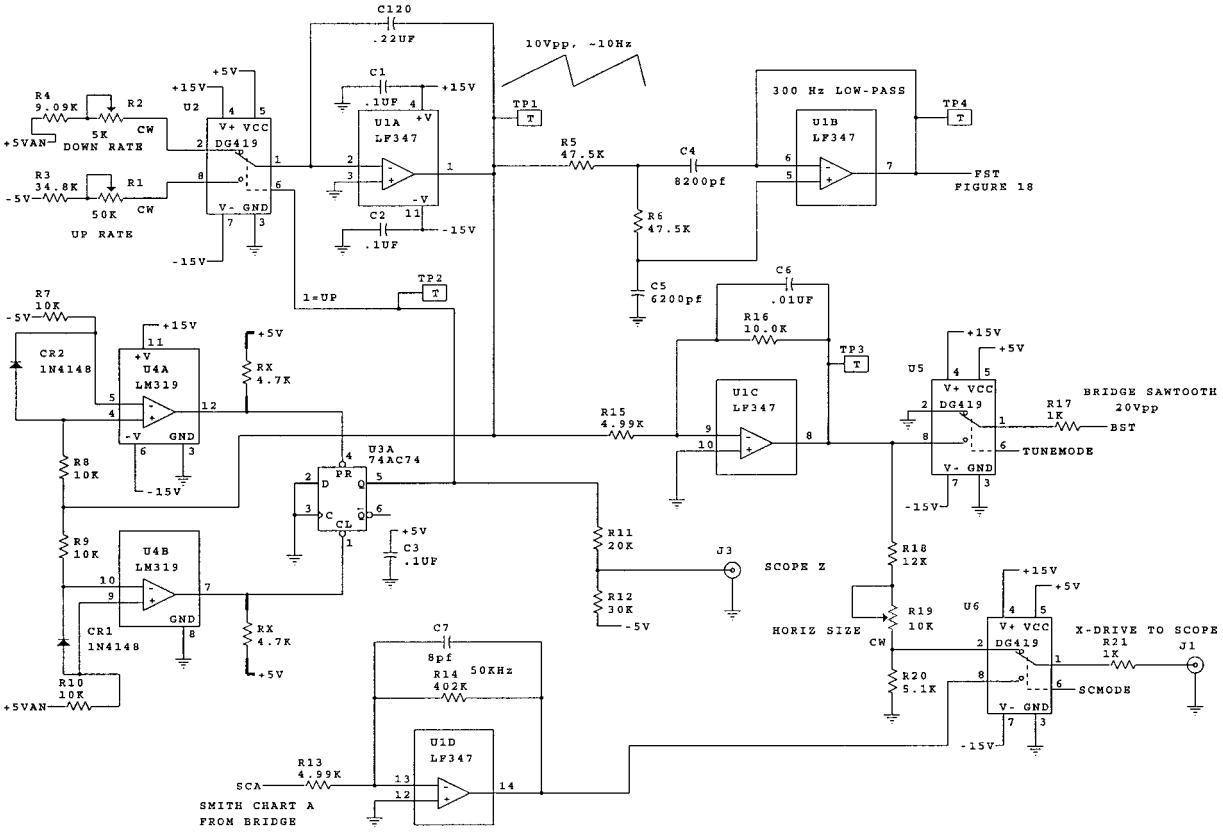

Figures 17 through 26 Schematic diagram of microprocessor-controlled interface unit circuit card containing circuits for linear sweep generation, 70 kHz null meter, field modulation control, slow field scan control, center field control, microprocessor and support chips, and serial communications interface.

modulation coils must be resonated as described in the sections on CW mode, because the inductance of the large coils is so high, but the DU modulation current control system uses the closed-loop calibration. An open-loop system would be used if the swept-frequency specification were removed.

The modulation system consists of the control system described here plus the power amplifier and modulation coils described below. The modulation control is a part of the microprocessor-based interface unit. Modulation control begins in Fig. 19. Stage U17 is a Hall effect sensing device through which the modulation coil current is routed. The output of this device is a voltage proportional to the current. This signal contains both the sinusoidal modulation component and the linear ramp component (~10 Hz). Stages U18A and U18C are a 3 kHz high-pass filter that attenuates the linear ramp component. This was designed at the time in which the minimum modulation frequency was to be 5 kHz. Stage U19 is the calibration and overall gain stage. Pot R44 is mounted on the front panel so that a calibration adjustment can be made to account for the modulation penetration into our large metal resonators. Note here that higher gain in this stage results in lower modulation amplitude. This is because this path is the negative feedback path of the control loop. Stages U20 and U22 are gain stages whose gain is set via the PC. The modulation amplitude is controlled in three ranges (0.01–0.1, 0.1–1, and 1–10 G_{pp}). The gains of these stages are set depending on which range the modulation amplitude requested by the user falls into. These three gain ranges effectively constitute the exponent of the desired modulation amplitude. The output of stage U22 goes to Fig. 26, which shows a full-wave balanced rectifier and peak detector. This circuit produces a DC voltage proportional to the peak-to-peak modulation current. At the lower edge of Fig. 21 is dual digital-to-analog (D/A) converter U28. Stage U28B converts a 12 bit number that represents the mantissa of the desired modulation amplitude, set by the user at the PC, into an analog voltage in the range of 0 to +5V. This voltage, indicated as "CMD" in the figure, is then sent to stage U55A (lower edge of Fig. 20). Stage

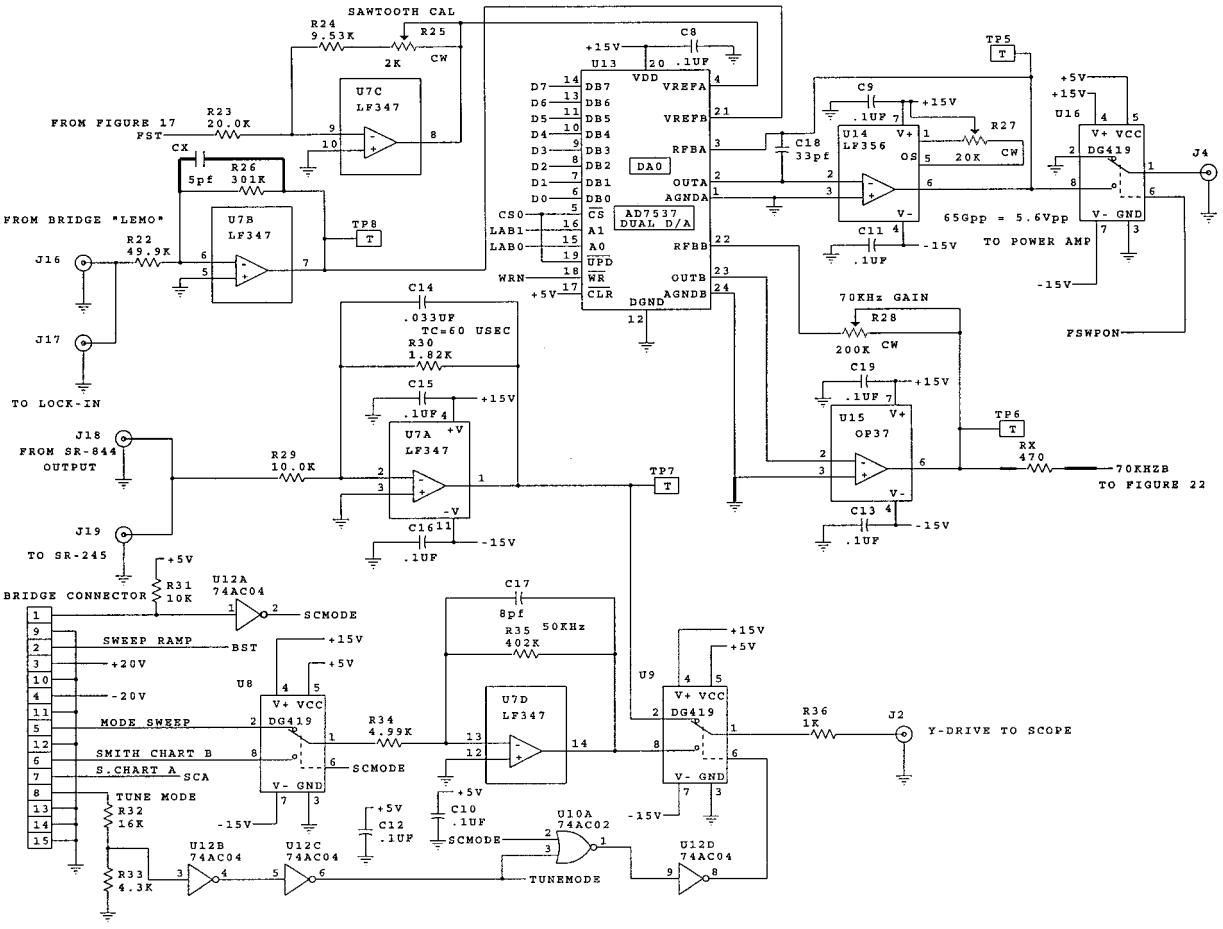

Figure 18

U55A subtracts the peak-detected DC voltage representing the measured modulation current from the command value to produce an error voltage. This error voltage is applied to variable gain stages U24A and U24B (Fig. 20, upper right). These stages amplify a sample of the sinusoidal modulation frequency being supplied from the HP 3310B function generator. This sinusoid comes into stage U55B as 1 V_{pp}, the level required to provide the lock-in amplifier reference. It is then attenuated by a resistive ladder and selected by U23A inversely in proportion to the modulation command exponent. Amplifiers U24A and U24B amplify the sinusoid up to the level necessary to force the error voltage to near zero. Very little steady-state error is required because the transfer function of U24A and U24B is linear in decibels or exponential voltage so the loop gain is very high. The output of U24B then goes through a scaling and impedance matching stage, U25C, and then out to the modulation power amplifier (see section below). Thus the loop is closed between a modulation command coming from the user via the PC and the measured modulation current. The difference, or error, is forced to near zero. The loop response time constant is set by the value of the low-pass filter formed by R76 and C49. This time constant is 3.6 s or an equivalent low pass corner at 43 mHz. This low-frequency response is necessary for stability given the high loop gain and the high Q of the resonant coil driver circuit.

Linear Ramp (Field Sweep) System. A relatively fast (compared to conventional slow scan data collection) linear field sweep is often useful in setting up the spectrometer by observing the spectrum on an oscilloscope. Our system provides a linear field sweep at ~10 Hz for this purpose. The ramp is produced by stage U1A (Fig. 17). The ramp is passed through stage U1B, a 300 Hz low-pass filter, to limit the upper harmonic content. Upper harmonic content must be suppressed so that it does not get through the 3 kHz high-pass filter described above and into the modulation feedback system. The ramp is then scaled by stage U7C (Fig. 18). Stages U13 and U14 provide 12 bit digital amplitude control. The digital value origi-

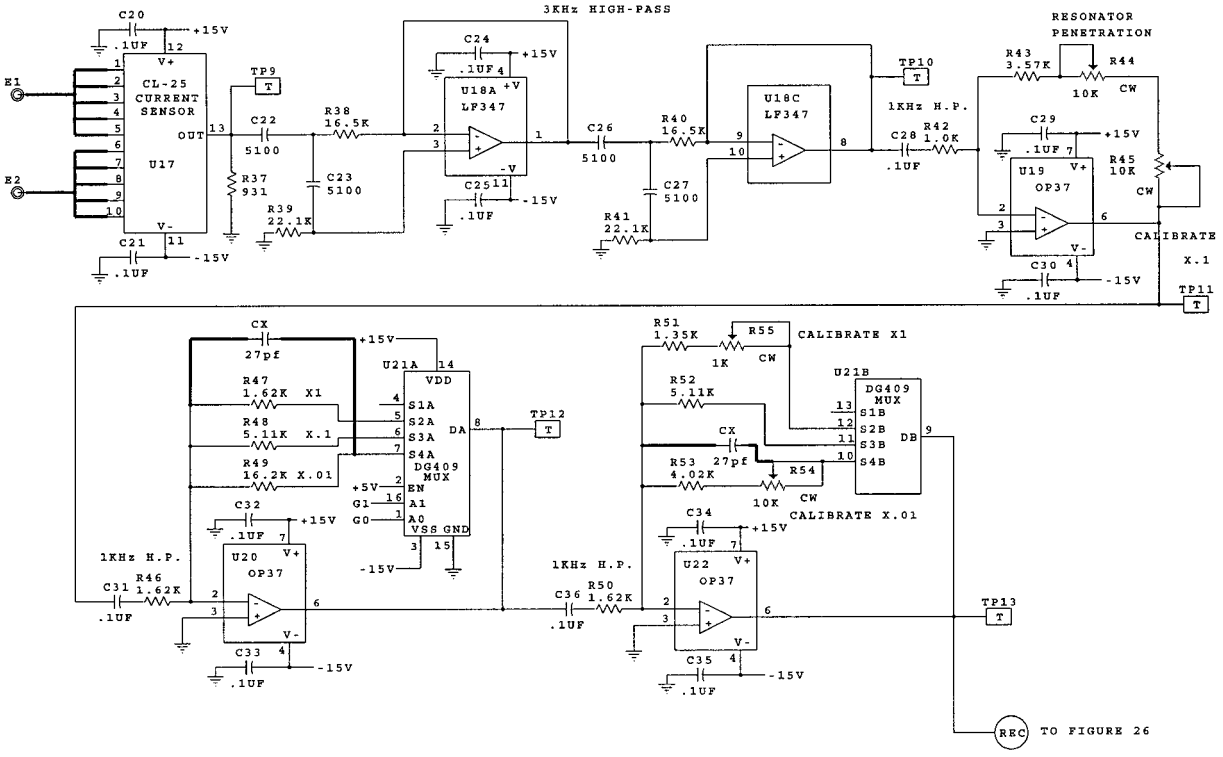

Figure 19

nates in the PC from a user setting of desired field sweep amplitude. The amplitude-adjusted ramp is then sent out to the linear sweep power amplifier (described below). It is important to trim out the DC offset in stage U14 (pot R27) because any DC offset will shift the center field. The linear sweep ramp is also used in resonator tuning modes to sweep the frequency of the RF source. Another use of the linear ramp in our system is to drive the *x* axis of the *x-y* oscilloscope display. This drive is provided through switch U6 (Fig. 17). Another part of the ramp system is the *z* drive (retrace blanking) to the *x-y* oscilloscope. This signal is derived from the up-down flip-flop U3A and sent to the *z* axis of the scope through connector J3.

Field Control in the DU System. **Center field control.** The center field is set by the user at the PC. This becomes a 12 bit value defining a center field over the range of 50 to 150 G. Stages U26B and U27B (Fig. 21) comprise a 12 bit D/A converter that produces a voltage analog of 0 to +10 V = 50 to 150 G (scale = 10 G/V). Stage 27C offsets and gain-adjusts this signal so that the scale is now 15 G/V. This stage also sums in contributions from the slow scan system (see below) and a center field front panel adjustment pot scaled by stage U55D. The front panel control can move the center field ±10 G. Stage U27D adds a microprocessor-controllable offset that can be used to compensate for any offset inherent in the magnet power supply. The scale factor at the output of U27D is 20 G/V with nominally zero offset. The signal now goes to Fig. 25 where stage U51B changes the scale to 100 G/V. This is the scale required by the HP power supply, which drives the 40 cm magnet (see below). Stage U51C rescales to 142 G/V, which is the scale required by the Kepco ATE supply that drives the 81 cm magnet. Switch U52 selects between the HP and the Kepco scale factors. This selection comes ultimately from the user at the PC. Switch U53 turns the center field on or off, again a selection of the user at the PC. The final output at J10 is cabled to either the HP or the Kepco power supply depending on which magnet is in use.

Slow field scan system. Stage U25A (Fig. 21) inverts the scan voltage arriving through connector J6 from the SR245 13 bit D/A converter. This was designed to be compatible with our previously designed software that controls our other spectrometers through SR245 interfaces. The slow scan software in the PC controls the SR245 over a serial communications port, which then provides a −10.24 to +10.23 voltage scan over the scan range selected. Stage U28A and U29A

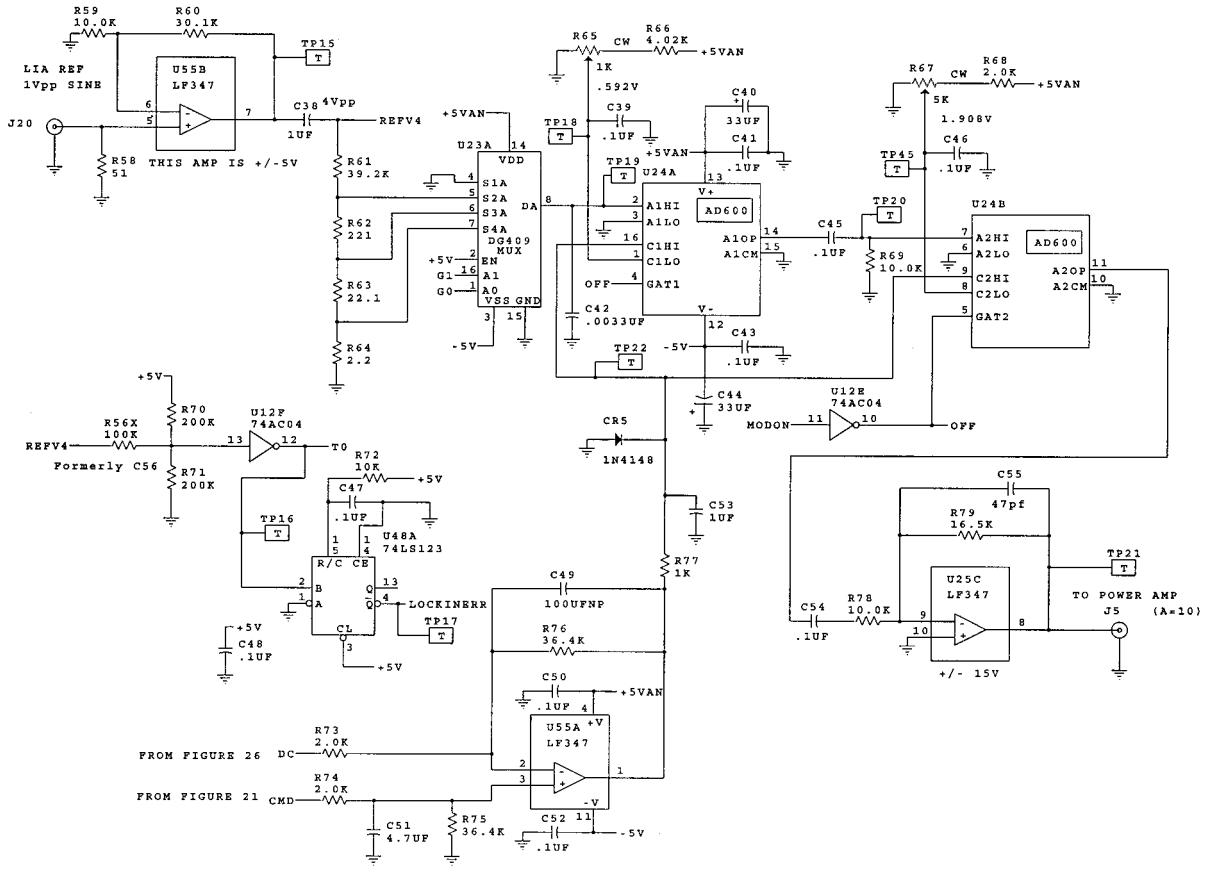

Figure 20

is a 12 bit inverting and multiplying D/A converter. The output of U29A is a voltage scan scaled to the selected scan range with a scale factor of 0.1023 V/G. The maximum scan range is 200 G (±100 G from center field) or ±10.23 V at the output of U29A. Switch U30 turns the slow scan system on or off, selectable by the user at the PC. The scaled scan voltage is then summed with the center field control voltage in stage U27C.

70 kHz phase tuning meter. Stage U7B (Fig. 18) acquires a sample of the bridge output that is passed through the microprocessor interface unit on its way to the lock-in amplifier (or Bruker signal channel). This sample contains both the EPR signal at the field modulation (lock-in reference) frequency and a component at the 70 kHz AFC modulation frequency. Since the EPR component is derived from an amplitude modulation (AM) component at the detecting mixer in the bridge, and the AFC is an FM component, they are in quadrature to one another. This allows setting the proper RF phase for absorption EPR without being able to observe an EPR signal. If the AFC component is nulled, this will be the best phase for absorption EPR (*58*). Stage U7B has a gain of ~6. This signal is then further scaled by a microprocessor-controlled multiplying D/A converter, stages U13B and U15. The output of this stage is synchronously detected by mixer U34 (Fig. 22). The 70 kHz reference comes from the bridge via connector J9 and is scaled by stage U33A. Stage U33D following the mixer provides a low-pass filter (corner frequency of 1.6 Hz) and a low impedance source for the next stage. Stages U33B and U33C constitute an absolute value amplifier, which then drives a front panel null meter. When the meter shows zero deflection the phase is properly tuned. Zener diode CR8 prevents overdrive of the meter when the phase is improperly tuned. This is a very sensitive and useful addition to the means of properly adjusting a CW EPR spectrometer.

***x-y* display drivers and Smith Chart amplifiers.** The resonator tuning display and the spectral display are on an *x-y* driven oscilloscope. The *x* axis is driven either by the field sweep ramp (spectral display), by

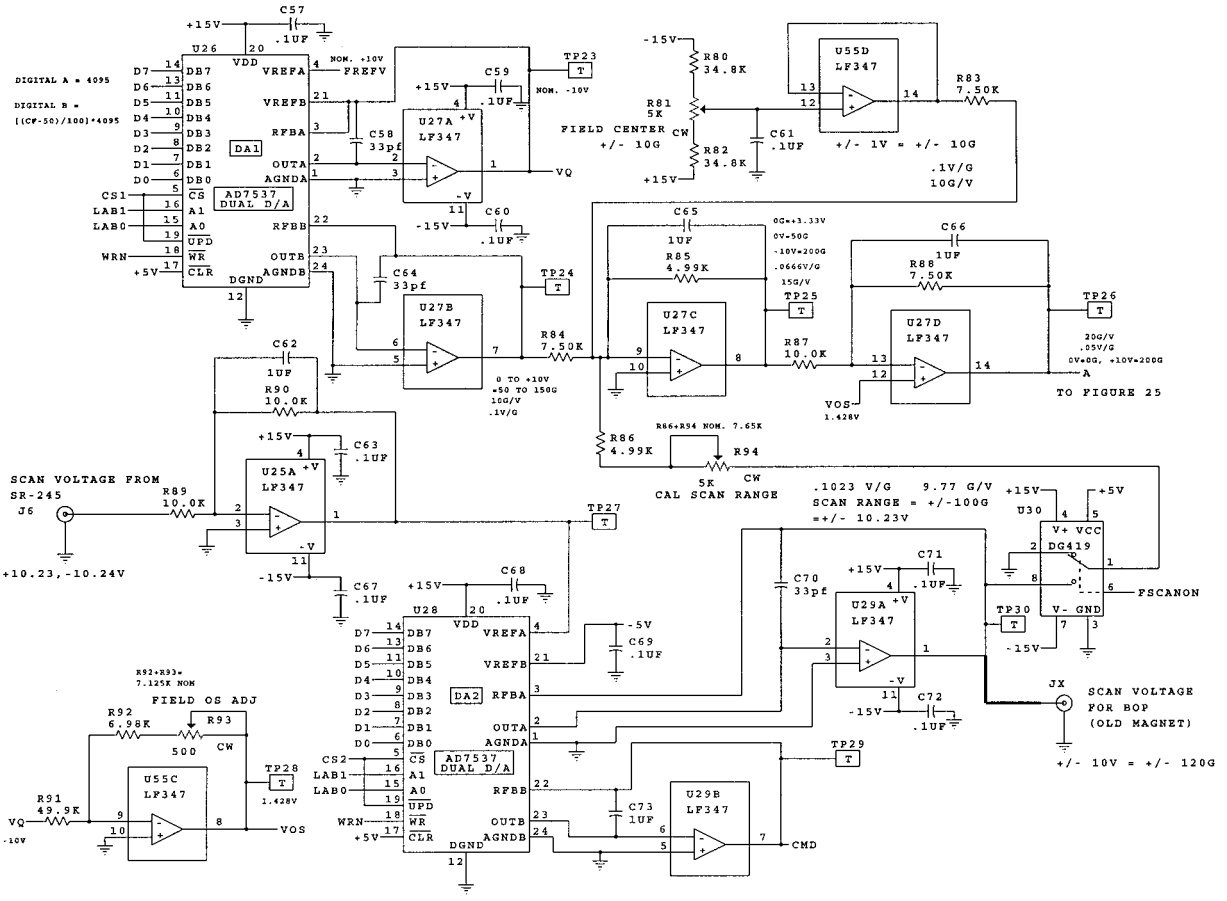

Figure 21

the source FM ramp (dip displays) or by one of the Smith Chart quadrature signals coming from the bridge (resonator tuning modes). Switch U6 (Fig. 17) makes this selection. Stage U1D amplifies the Smith chart signal coming from the bridge before it is applied to the *x* axis of the scope. The *y* axis (lower portion of Fig. 18) is selected by switches U8 and U9 to come from either the lock-in output (spectral display), the mode sweep signal from the bridge (dip displays), or the other Smith Chart mixer that is in quadrature to the one supplying the *x* axis drive in the Smith Chart mode. This signal and the mode sweep signal are amplified by stage U7D. The *z* axis (retrace blanking) is derived from the ramp generator circuit (U3A).

8051 microprocessor and serial communications interface. Figure 23 shows 80C31 microprocessor U35 and support chips. The 80C31 is one in the generic family of 8051 8 bit microprocessors made by Intel, Maxim, Philips, and others. U38 decodes chip selects for peripheral devices such as D/A converters and the communications port. U40 is a ultraviolet-erasable EPROM that contains the microprocessor object code. RAM chip U41 provides for temporary storage of variables, but this socket has not been used yet because the on-board RAM of the microprocessor proved sufficient. The source code was written in 8051 Assembler language and initially tested and developed using Signum Systems model USP-51 in-circuit emulator. The source code is ~550 lines of 8051 assembly language code (available from the authors). The microprocessor receives instructions and parameters over a serial communications port from the PC at 9600 baud. The protocol for this communication is defined in a document available from the authors. UART chip U42 (Fig. 24) receives control parameters from, and sends status parameters to, the PC. The UART generates interrupts to the microprocessor to process incoming and outgoing data bytes. One-shot U47B (Fig. 23) blinks a front panel light indicating communications activity. The microprocessor runs at 10 MHz formed by oscillator U50 and divider U3B (Fig. 24).

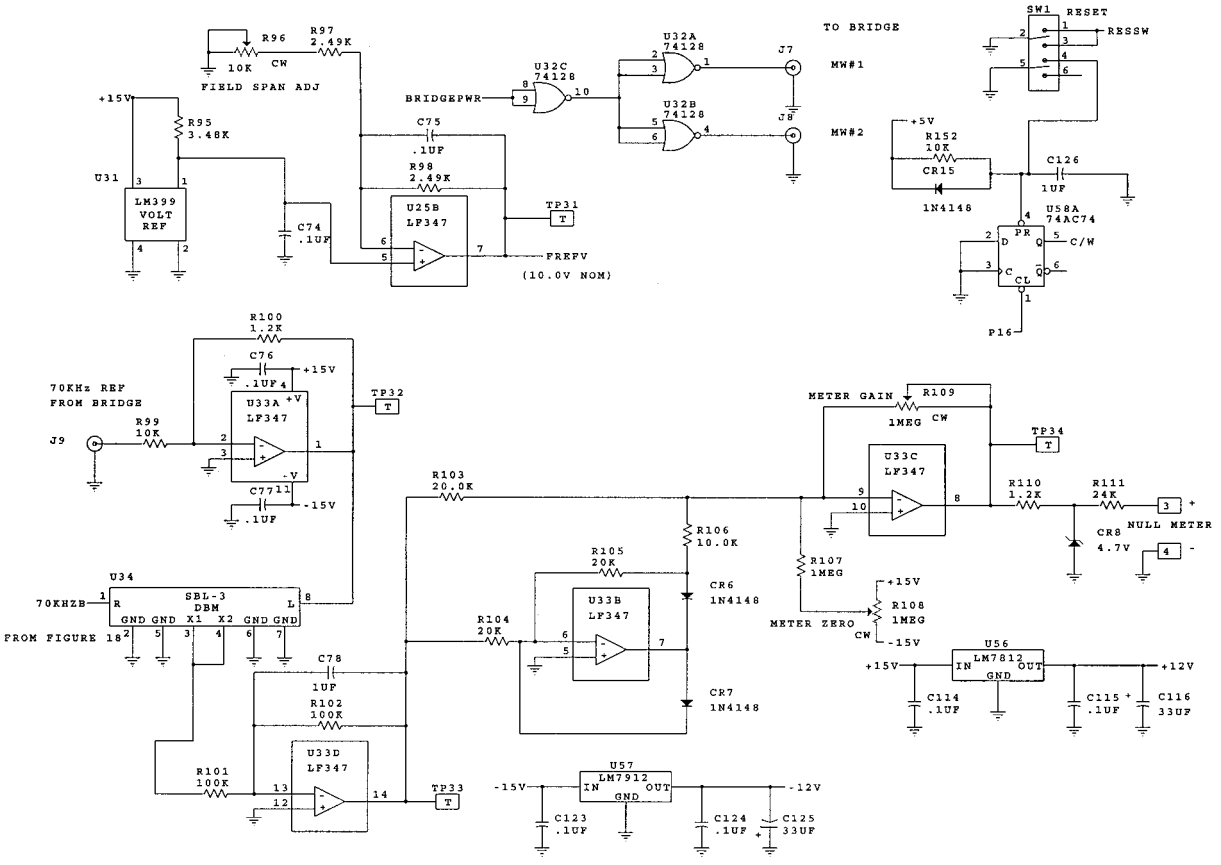

Figure 22

Lock-In Amplifier

We currently use two different lock-in amplifiers depending on the field modulation frequency. At 19 kHz we use an analog type, Stanford Research model SR510, and at 45 kHz we use a digital lock-in, Stanford Research model SR844. The SR844 does not operate below 25 kHz. These units provide phase-sensitive detection at the field modulation frequency, adjustable gain and final signal filtering before being digitized. We digitize the output of either lock-in using a Stanford Research model SR245 digitizer, but we could also obtain digital information directly from the SR844. We have not implemented this feature.

Modulation Power Amplifier

The modulation power amplifier (Fig. 27) is based on an Apex model PA05 power op-amp. This amplifier has a gain-bandwidth product of 400 kHz when driving a 4Ω load and can drive loads of up to 10 A with up to 40 V. We used the large heat sink and printed circuit board supplied by Apex (EK04). We set the gain at 10×, which is sufficient to drive the 7 inch (17.8 cm) modulation coils when resonated with a series capacitor. Figure 27 shows the resonating capacitor selection switch, which is on the front panel of the unit. There is also a current reversing switch that can compensate for mounting the modulation coils in the main magnet in either of two possible orientations. Inductor L1 is locally constructed. It is wound with no. 12 AWG magnet wire on a laminated iron core. An air gap was inserted to prevent saturation from the (nearly) DC current. The inductance is ~31 mH. This inductor isolates the sinusoidal modulation system from the low-frequency linear sweep system.

Linear Sweep Power Amplifier

The linear sweep power amplifier (Fig. 28) is a current mode amplifier of local design and construction. Current is sensed by resistor R9, and U1B produces a voltage proportional to current of 0.5 V/A. This is the feedback to the main driver stage U1A so the transfer function of the entire power amplifier is 2 A/V. The

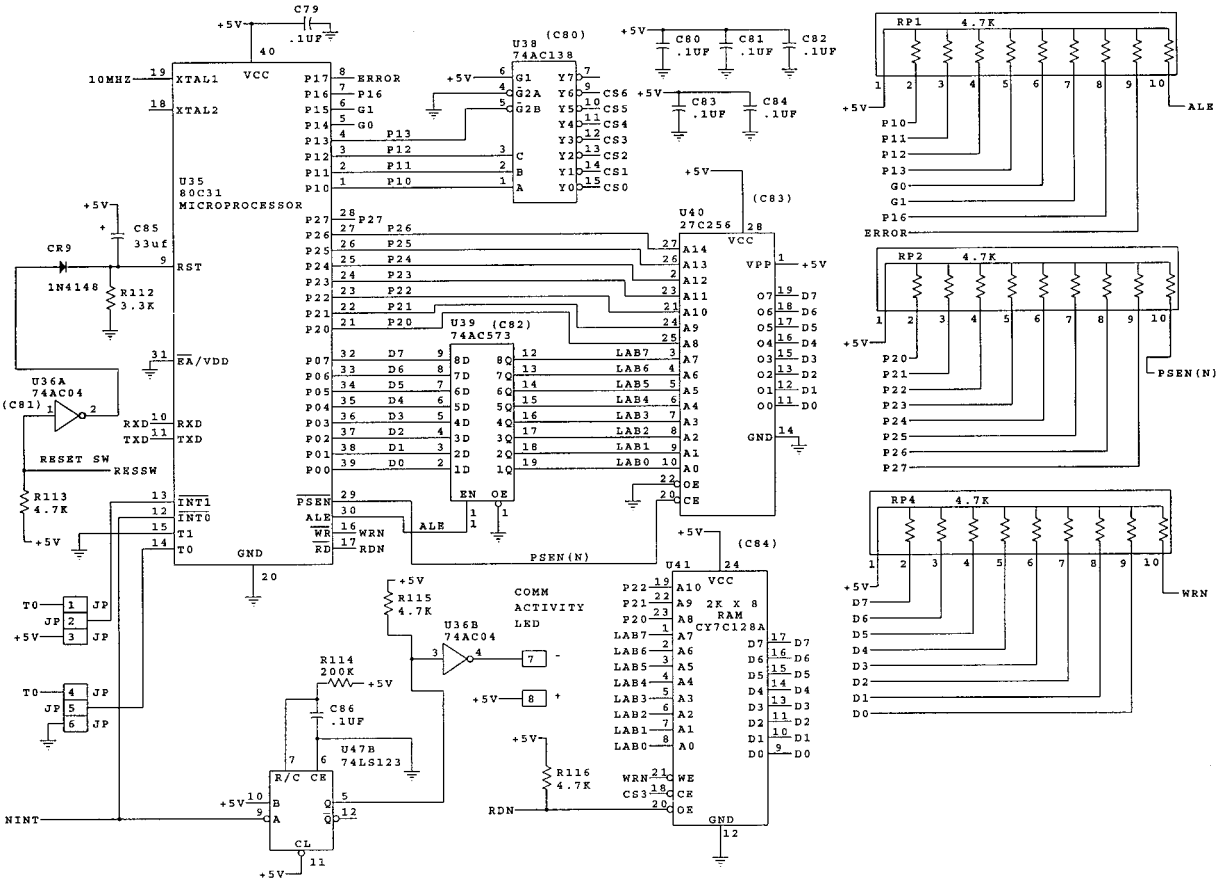

Figure 23

modulation coils have a field constant of ~7.5 G/A so a 60 G_{pp} field sweep requires ~8 A pp or ~4 V_{pp} at the input to the power amplifier.

Modulation Coils

The modulation coils are of local design and construction. The coils currently in use are wound on machined plexiglas forms with an average winding diameter of 17.8 cm. Each coil is 75 turns of no. 14 AWG varnished magnet wire. The total inductance of both coils in series and approximately 12 ft of twisted lead feed wire is ~2.8 mH. The measured field constant at the center for Helmholtz spacing is 7.52 G/A. Because of our large resonators we have to mount the coils at greater than Helmholtz spacing, which results in ~10–15% reduction in the field constant. The resonators also have only fractional penetration so we have calibrated the modulation amplitude at the sample by empirical methods.

Bruker to Kepco Interface Circuit for Field Control

The interface unit shown in Figs. 2 and 4 between the Bruker field controller and the magnet power supply (Kepco model ATE 36–30M) is required to match the transfer function of the power supply and magnet to the Bruker. The Bruker field controller was designed to control a power supply with a large gain and driving an iron-core magnet with a large time constant. The interface circuit (Fig. 29) provides the gain and time constant required to stabilize the control loop. Stage U1A provides gain of ~10 and R4, R5, and C4 provide the time constant of ~30 s. U1C provides a summing junction to bring in a rapid scan control voltage that bypasses the large time constant. This is useful to scan the magnet rapidly in certain types of experiments.

System Power Supplies

In a system this large and complex a rather large number of different power supply voltages are re-

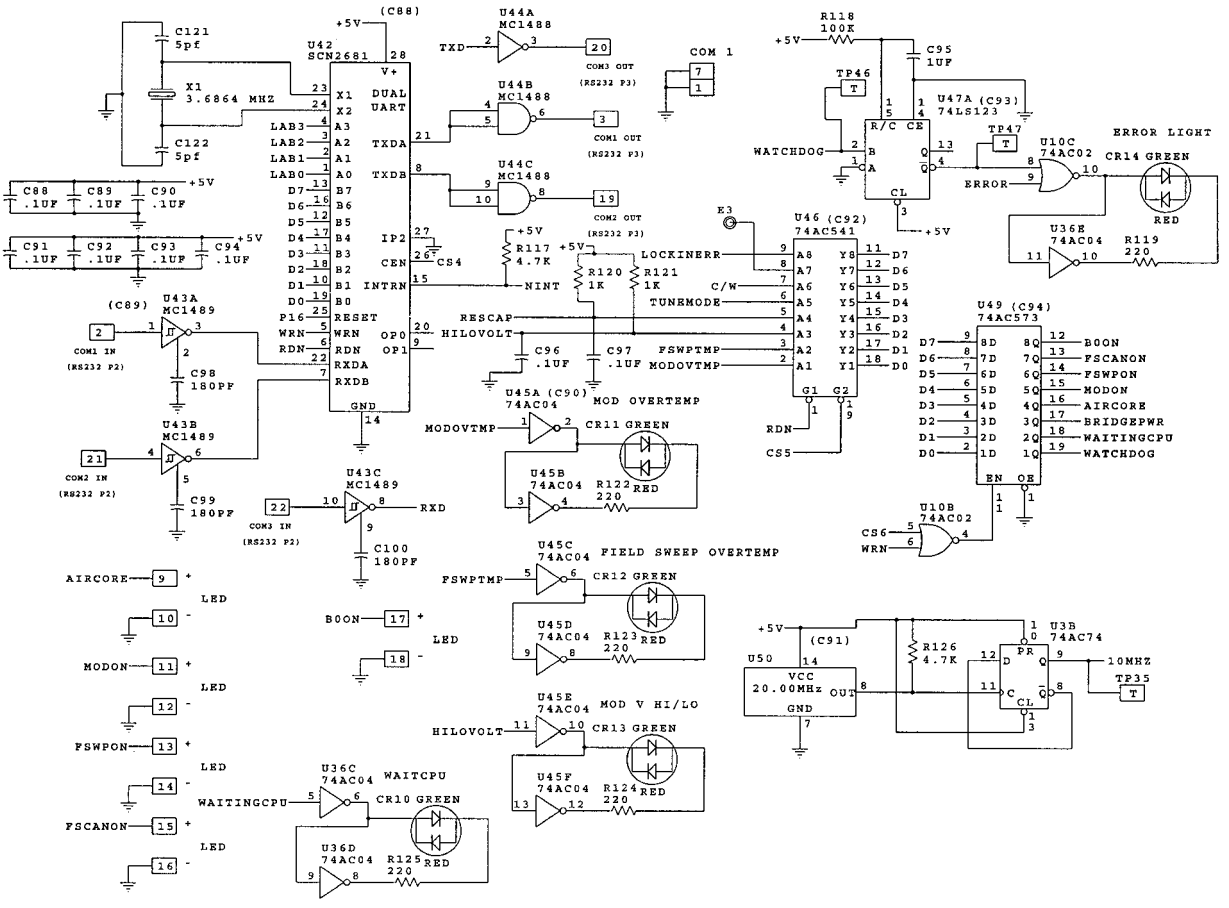

Figure 24

quired. A total of 12 different DC voltages were required ranging from ±48 V for the modulation power amplifier to ±5 V for some op-amps. Another requirement was to make the bridge compatible with Varian E-Line X-band bridges, which operate on ’f120 V. The power supplies were constructed from commercially available units and packaged into larger boxes with alternating current power fuses and on-off switches.

RESULTS AND DISCUSSION

In the following paragraphs we comment on experience to date with the RF source, the resonator, the magnet, and CW and pulse operation. Other than the bridge and resonator, there are two complete spectrometers, one locally constructed and one based on the Bruker E540 console. As the spectrometer has developed, it has been convenient to have locally designed and constructed modules for all functions of the spectrometer, so that components can be changed to test hypotheses about performance. When an aspect is well developed, it becomes convenient to transfer that function to the Bruker hardware and software system. For example, at this stage we routinely acquire FIDs with the SpecJet hardware and Xepr software. The magnetic field is controlled by the Bruker ER032T field control system, which uses a Hall probe. The device developed to use this to control the current in the air-core magnet is described in an accompanying paper (*59*).

Numerous CW and pulsed EPR spectra have been run to test the functions of the spectrometer and challenge its performance. Some FIDs and spin-echo measurements of relaxation times obtained with the spectrometer are presented in Ref. *40*. The sample was a 0.2 mM aqueous solution of the deuterated symmetric trityl and the trityl called OX-31, both synthesized by Nycomed (*53*). The samples contained $\sim 4.6 \times 10^{17}$ spins in a 10 mm outside diameter (o.d.) NMR tube. A larger sample could have been used, since the aqueous sample causes only a small reduction of resonator Q at 250 MHz. The echo signal in

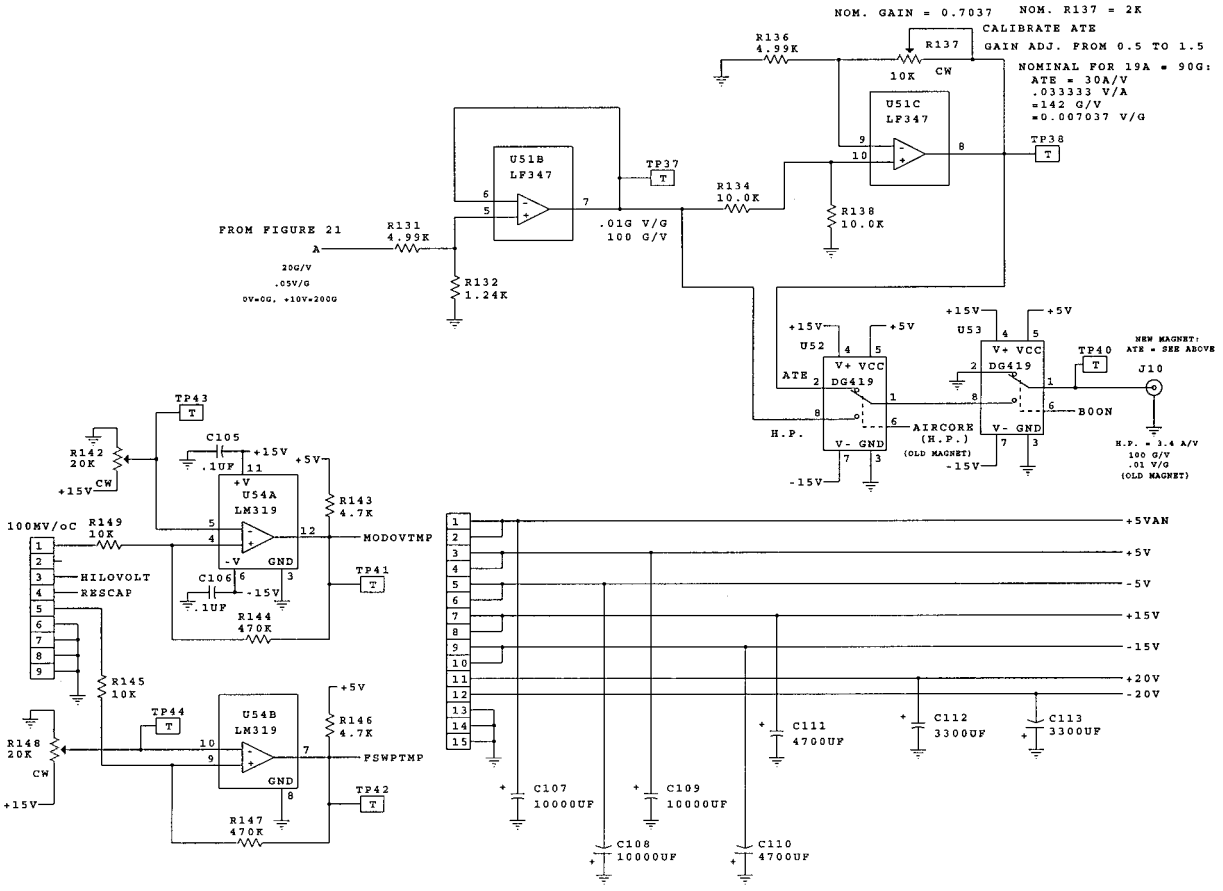

Figure 25

Fig. 8 of Ref. *40*, obtained by accumulating 99,328 echoes in 13.4 s using the Bruker SpecJet digitizer, had S/N = 396. The pulse repetition rate was limited by the long relaxation time of this species. The CLR was overcoupled as described in Ref. *40*, and the echo signal was amplified by the Berkshire amplifier close

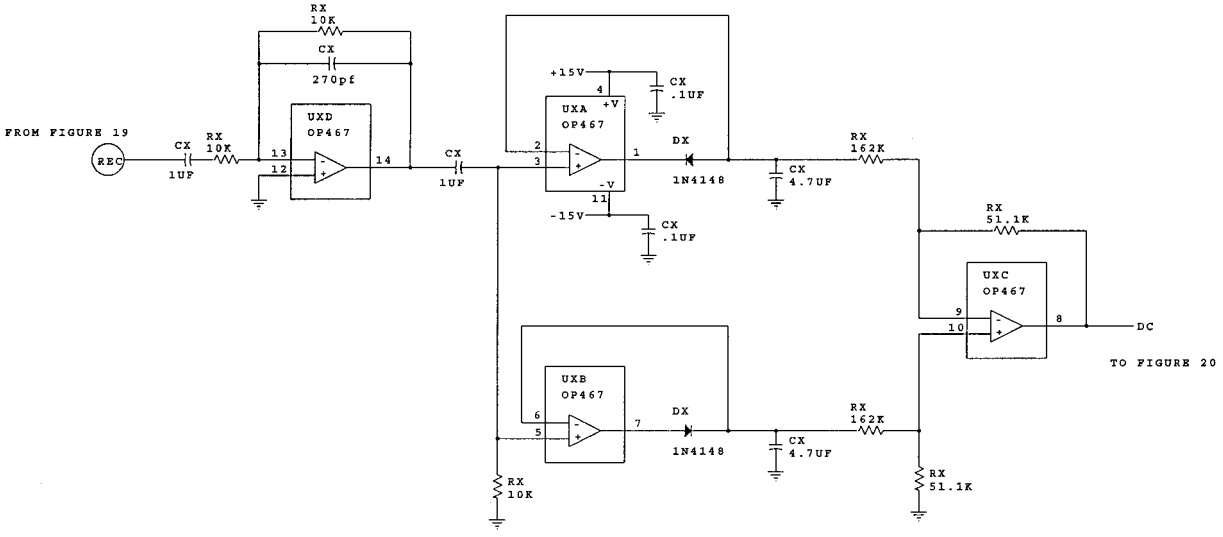

Figure 26

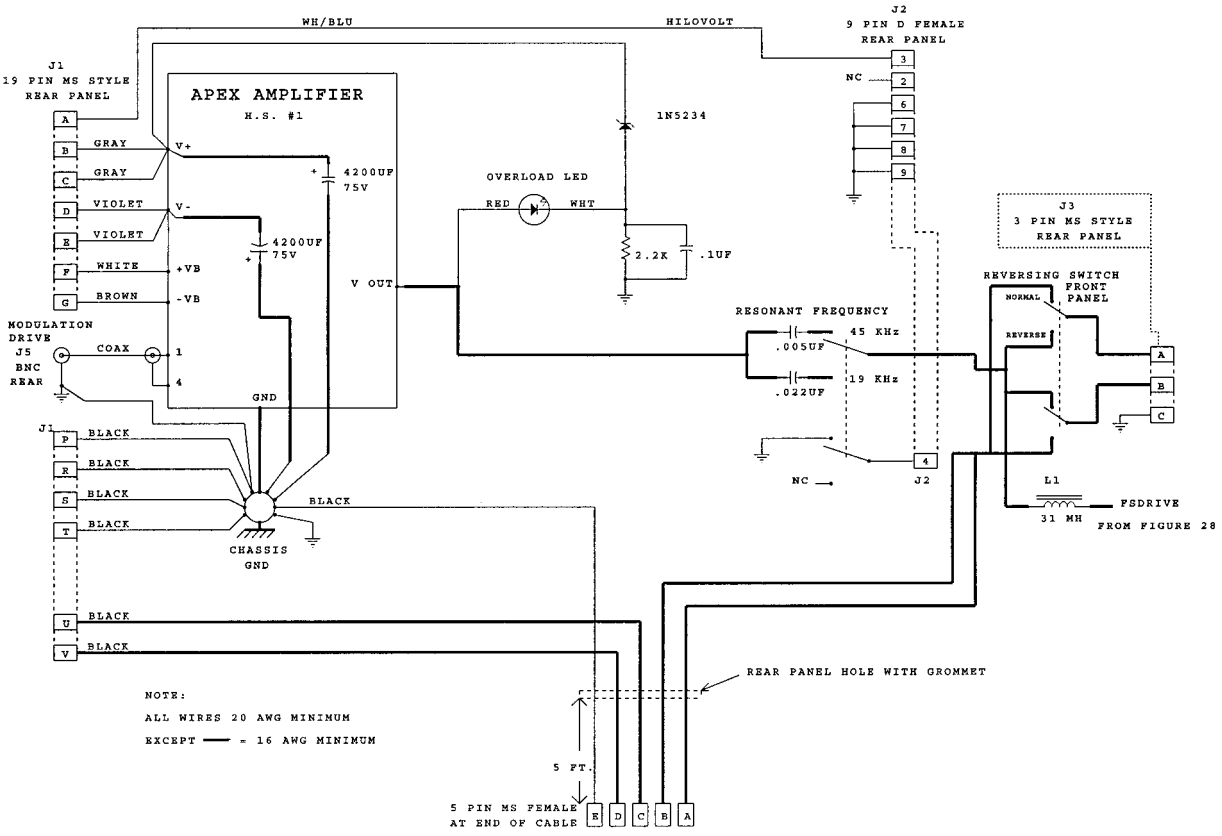

Figure 27 Schematic diagram of modulation power amplifier.

to the CLR, as described above. By extrapolation, it can be estimated that 4.3×10^{15} spins with the same relaxation time could be detected with S/N = 1 in 1 s. We observed a slope in the baseline of field-swept spectra and found that it was due to magnetic field interaction with the circulator and isolator in the bridge. The circulator was shielded in a $6 \times 3.5 \times 2.5$ inch box constructed of MμMetal by MμShield Company, Inc. (Goffstown, NH, drawing S2751). The isolator was shielded with a homemade steel shield. The shielding of these components and careful positioning of the magnet relative to the bridge minimized the baseline slope.

For pulsed EPR it is necessary to amplify the source RF. One approach is to use a CW amplifier, pulse the input, and use extensive signal averaging to reduce the noise that is output by the RF amplifier during the signal detection period. For our initial testing, we have done this, using a Dressler 75 W CW class A amplifier, which at ~250 MHz delivers ~20 W to the resonator. FIDs have been observed for Nycomed trityl and lithium phthalocyanine radicals, and spin echoes have been observed for trityl and irradiated SiO_2.

We have used several different style resonators at 250 MHz. A small five-turn coil sized for 4 mm o.d. tubes, similar to an NMR resonator, was used for mapping the magnetic field with small samples. A LGR that holds a 1 inch (25 mm o.d.) sample tube analogous to the LGRs we have used previously at higher frequencies (*49*) has been used for CW spectra with magnetic field modulation. A CLR analogous to those we used at S-band and L-band, but large enough to hold a 1-inch o.d. sample tube has been used for pulsed EPR, where the isolation is important (*40*).

This spectrometer incorporates two air-core magnets. One has four coils of the same diameter, with a cylindrical sample space of ~40 cm diameter. The other magnet, described in Ref. *60*, is about twice the diameter and achieves a 15 cm diameter homogeneous volume. This magnet also incorporates magnetic field gradient coils for three-dimensional imaging.

EPR signals are inherently weak and are especially weak at such a low RF frequency. Consequently, the spectrometer has many gain stages, selectable for the type of measurement. As shown in Figs. 3 and 4, the signal from a CLR can be amplified immediately, but

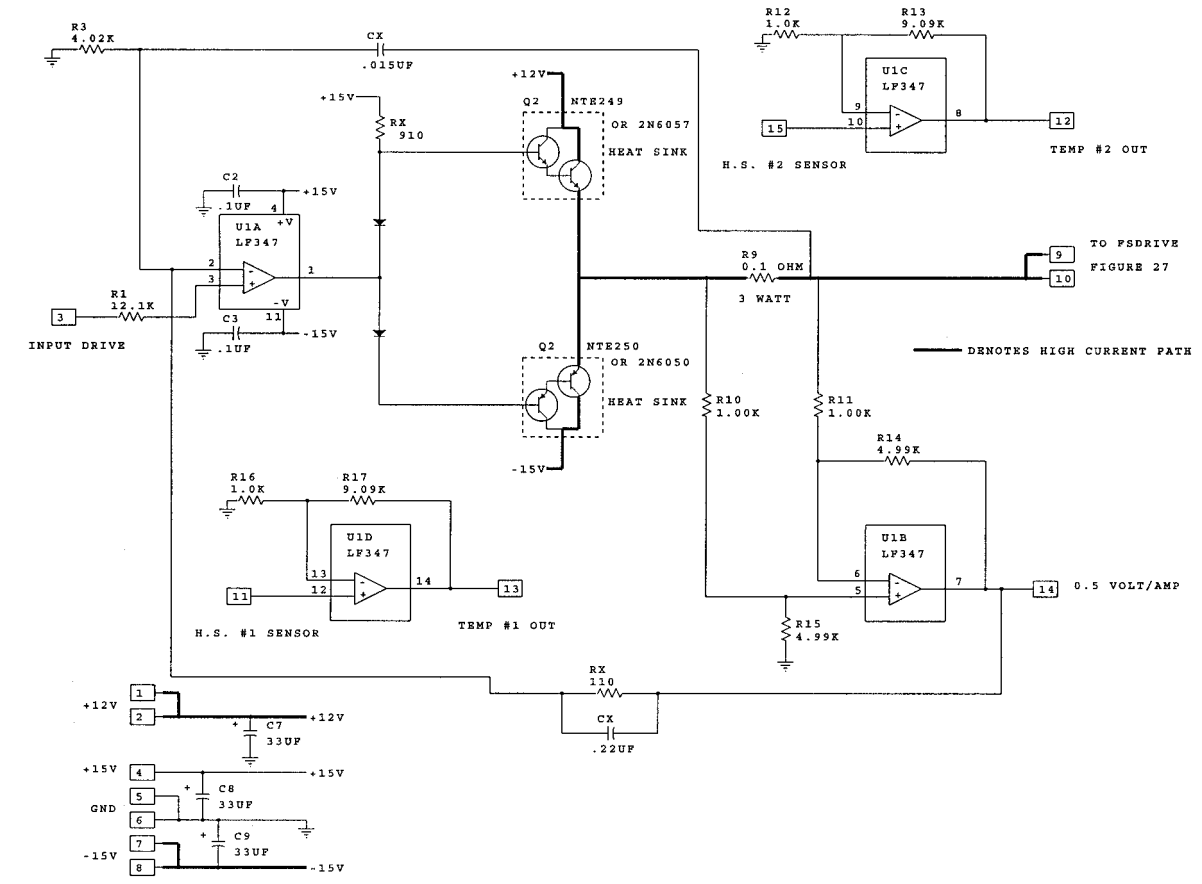

Figure 28 Schematic diagram of linear sweep power amplifier.

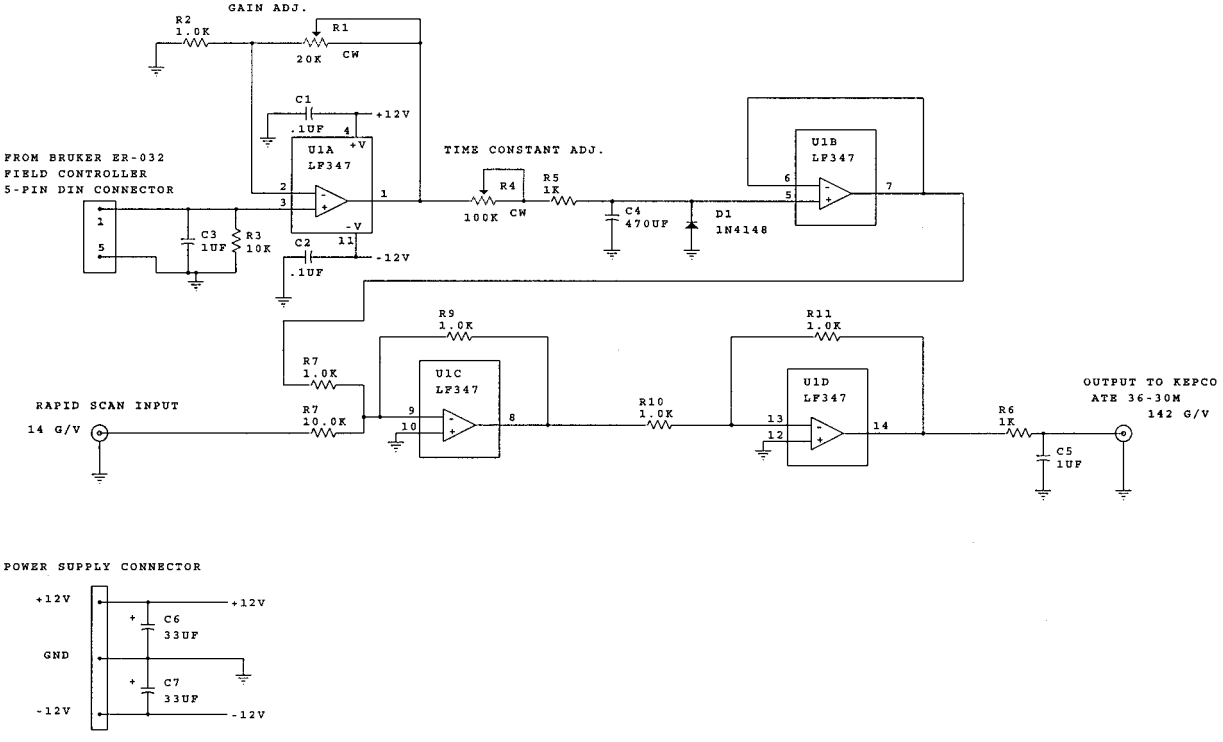

Figure 29 Schematic diagram of Bruker to Kepco magnet power supply interface.

the signal from a LGR can be amplified only after it has passed through the circulator. With high-incident RF power, the power reflected from a LGR could saturate one of the amplifier stages if maximum available amplification were used, so several options are available. Baseline drift is a potential problem in both CW and pulsed measurements, so we commonly use less than the maximum gain one might expect to be able to use to avoid reaching the limit of some stage during long-time averaging.

The detection system of the pulse bridge includes pulse amplifiers, locally designed and constructed, with selectable gains that have been interfaced to the SpecJet high-speed digitizer in the Bruker E540 console, which has ± 0.5 V full scale input dynamic range. The SpecJet provides dual-channel digitization and high-speed averaging capability (*61*). Presently we are doing the high-speed timing control with our locally designed PTU (*54–56*), with plans to eventually use the Bruker PatternJet timing system.

The spectrometer described has achieved the goal of facilitating testing of both LGR and CLR in CW and pulse operation with two magnets and multiple power supply combinations. The FID signal amplitude agrees with prediction based on the properties of the resonator and the measured overall gain of the detection system and agrees with predictions as a function of RF/microwave frequency (*49*).

Further development is planned of enhancements in resonators to decrease dead time and of improvements in RF power amplifiers to increase pulse power and decrease dead time. It is also planned to place a CLR and first-stage amplifier in a cryostat, and cool them to liquid He temperatures for echo envelope modulation studies of proteins.

If only one of the functions built into this bridge is needed (e.g., CW with reflection resonator or pulse with CLR), the bridge could be simplified considerably.

ACKNOWLEDGMENTS

A generous gift of trityl radical from Nycomed Innovations AB to Professor Howard J. Halpern (Chicago) facilitated this research. Initial construction of the prototype CW bridge and the 40 cm diameter magnet was funded by National Science Foundation STTR Grant DMI-9523205 to Omni Engineering and the University of Denver in 1995. Design and construction of the resonators used in Denver was supported by National Institutes of Health Grants RR12183 and GM57577 (G.A.R.). The pulsed spectrometer design and development was supported by National Institutes of Health Grant P41 RR12257 (H.J.H. and G.R.E.) and by Bruker BioSpin EPR Division and the University of Denver.

REFERENCES

1. Eaton GR, Eaton SS. EPR spectrometers at frequencies below X-band. Biol Magn Reson, in press.
2. Eaton SS, Eaton GR. Relaxation times of organic radicals and transition metal ions. In: Eaton GR, Eaton SS, Berliner LJ, editors. Distance measurements in biological systems by EPR. Biol Magn Reson 2000; 19:29–154.
3. Swartz HM, Halpern H. EPR studies of living animals and related model systems (in vivo EPR). In: Berliner LJ. Spin labeling: the next millennium. Biol Magn Reson 1998; 14:367–404.
4. Greenslade DJ, Koptyug AV, Symons MCR. Aspects of low-frequency low-field electron spin resonance. Roy Soc Chem Annu Rep C 1996; 92:3–21.
5. Halpern HJ, Spencer DP, van Polen J, Bowman MK, Nelson AC, Dowey EM, Teicher BA. Imaging radio frequency electron-spin-resonance spectrometer with high resolution and sensitivity for in vivo measurements. Rev Sci Instrum 1989; 60:1040–1050.
6. Halpern, HJ, Bowman MK. In: Eaton GR, Eaton SS, Ohno K, editors. EPR imaging and in vivo EPR. Boca Raton, FL: CRC Press; 1991. p 45–63.
7. Brivati JA, Stevens AD, Symons MCR. A radiofrequency spectrometer for in vivo imaging. J Magn Reson 1991; 92:480–489.
8. Stevens AD, Brivati JA. A 250 MHz EPR spectrometer with rapid phase-error correction for imaging large biological specimens. Meas Sci Technol 1994; 5:793–796.
9. Symons MCR. Whole body electron spin resonance imaging spectrometer. In: Ohya-Nishiguchi H, Packer L, editors. Bioradicals detected by ESR spectroscopy. Basel: Birkhauser Verlag; 1995. p 93–102.
10. Bourg J, Krishna MC, Mitchell JB, Tschudin RG, Pohida TJ, Friauf WS, Smith PD, Metcalfe J, Harrington F, Subramanian S. Radiofrequency FT EPR spectroscopy and imaging. J Magn Reson B 1993; 102:112–115.
11. Pohida TJ, Fredrickson HA, Tschudin RG, Fessler JF, Krishna MC, Bourg J, Harrington F, Subramanian S. High-speed digitizer/averager data-acquisition system for Fourier transform electron paramagnetic resonance spectroscopy. Rev Sci Instrum 1994; 65:2500–2504.
12. Murugesan R, Cook JA, Devasahayam N, Afeworki M, Subramanian S, Tschudin R, Larsen JA, Mitchell JB, Russo A, Krishna MC. In vivo imaging of a stable paramagnetic probe by pulsed-radiofrquency electron paramagnetic resonance spectroscopy. Magn Reson Med 1997; 38:409–414.
13. Murugesan R, Afeworki M, Cook JA, Devasahayam N, Tschudin R, Mitchell JB, Subramanian S, Krishna MC.

A broadband pulsed radio frequency electron paramagnetic resonance spectrometer for biological applications. Rev Sci Instrum 1998; 69:1869–1876.
14. Rubinson KA, Cook JA, Mitchell JB, Murugesan R, Krishna MC, Subramanian S. FT-EPR with a nonresonant probe: use of a truncated coaxial line. J Magn Reson 1998; 132:255–259.
15. Subramanian S, Murugesan R, Devasahayam N, Cook JA, Afeworki M, Pohida T, Tschudin RG, Mitchell JB, Krishna MC. High-speed data acquisition system and receiver configurations for time-domain radiofrequency electron paramagnetic resonance spectroscopy and imaging. J Magn Reson 1999; 137:379–388.
16. Afeworki M, Gooitzen MvD, Devasahayam N, Murugesan R, Cook J, Coffin D, A-Larsen JH, Mitchell JB, Subramanian S, Krishna MC. Three-dimensional whole body imaging of spin probes in mice by time-domain radiofrequency electron paramagnetic resonance. Magn Reson Med 2000; 43:375–382.
17. Devasahayam N, Subramanian S, Murugesan R, Cook JA, Afeworki M, Tschudin RG, Mitchell JB, Krishna MC. Parallel coil resonators for time-domain radiofrequency electron paramagnetic resonance imaging of biological objects. J Magn Reson 2000; 142:168–176.
18. Blume RJ. Electron spin relaxation times in sodium-ammonia solutions. Phys Rev 1958; 109:1867–1873.
19. Sachs G, Stöcklein W, Bail B, Dormann E, Schwoerer M. Electron spin relaxation of new organic conductors: fluoranthenyl radical cation salts. Chem Phys Lett 1982; 89:179–182.
20. Sachs G, Dormann E. Low field pulsed electron spin resonance in organic conductors. Bruker Report; 1984. p 30.
21. Callaghan PT, Coy A, Dormann E, Ruf R, Kaplan N. Pulsed-gradient spin-echo ESR. J Magn Reson A 1994; 111:127–131.
22. Coy A, Kaplan N, Callaghan PT. Three-dimensional pulsed ESR imaging. J Magn Reson A 1996; 121:201–205.
23. Wokrina T, Dormann E, Kaplan N. Conduction-electron spin relaxation and diffusion in the radical cation salt diperylene hexafluorophosphate. Phys Rev B 1996; 54:10492–10501.
24. Dormann E, Sachs G, Stöcklein W, Bail B, Schwoerer M. Gaussmeter application of an organic conductor. Appl Phys A 1983; 30:227–231.
25. Alexandrowicz G, Tashma T, Feintuch A, Grayevsky A, Dormann E, Kaplan N. Spatial mapping of mobility and density of the conduction electrons in $(FA)_2PF_6$. Phys Rev Lett 2000; 84:2973–2976.
26. Feintuch A, Alexandrowicz G, Tashma T, Boasson Y, Grayevsky A, Kaplan N. Three-dimensional pulsed ESR Fourier imaging. J Magn Reson 2000; 142:382–385.
27. Alecci M, Brivati JA, Placidi G, Sotgiu A. A radiofrequency (220 MHz) Fourier transform EPR spectrometer. J Magn Reson 1998; 130:272–280.
28. Alecci M, Brivati JA, Placidi G, Test L, Lurie DJ, Sotgiu A. A Submicrosecond resonator and receiver system for pulsed magnetic resonance with large samples. J Magn Reson 1998; 132:162–166.
29. Nishigawa H, Fujii H, Berliner LJ. Helices and surface coils for low field in vivo ESR and EPR imaging applications. J Magn Reson 1985; 62:79–86.
30. Berliner LJ, Fujii H. Magnetic resonance imaging of biological specimens by electron paramagnetic resonance of nitroxide spin labels. Science 1985; 227:517–519.
31. Fujii H, Berliner LJ. One- and two-dimensional EPR imaging studies on phantoms and plant specimens. Magn Reson Med 1985; 2:275–282.
32. Koscielniak J, Berliner LJ. Dual diode detector for homodyne EPR microwave bridges. Rev Sci Instrum 1994; 65:2227–2230.
33. Nilges MJ, Walczak T, Swartz HM. 1 GHz in vivo ESR spectrometer operating with a surface probe. Phys Med 1989; 2–4:195–201.
34. Froncisz W, Hyde JS. The loop-gap resonator: a new microwave lumped circuit ESR sample structure. J Magn Reson 1982; 47:515–521.
35. Hyde JS, Froncisz W. Loop gap resonators. In: Hoff AJ, editor. Advanced EPR: applications in biology and biochemistry. Amsterdam: Elsevier; 1989. p 277–306.
36. Rinard GA, Quine RW, Ghim BT, Eaton SS, Eaton GR. Easily tunable crossed-loop (bimodal) EPR resonator. J Magn Reson A 1996; 122:50–57.
37. Rinard GA, Quine RW, Ghim BT, Eaton SS, Eaton GR. Dispersion and superheterodyne EPR using a bimodal resonator. J Magn Reson A 1996; 122:58–63.
38. Rinard GA. Crossed-loop resonator structure for spectroscopy. US Patent 5,739,690; 1998.
39. Rinard GA, Quine RW, Eaton GR. An L-band crossed-loop (bimodal) resonator. J Magn Reson 2000; 144:85–88.
40. Rinard GA, Quine RW, Eaton GR, Eaton SS. 250 MHz crossed-loop resonator for pulsed electron paramagnetic resonance. Concepts Magn Reson 2002; 15:49–58.
41. Sotgiu A, Gualtieri G, Momo F, Indovina PL. ESR imaging: an overview. Phys Med 1988; 3/4:149–183.
42. Alecci M, Gualtieri G, Sotgiu A, Testa T, Varoli V. Multipolar magnet for low-frequency ESR imaging. Meas Sci Technol 1991; 2:32–37.
43. Alecci M, Penna, SD, Sotgiu A, Test A. R.F. (280 MHz) EPR imaging of extended samples: apparatus and preliminary results. Appl Magn Reson 1992; 3:909–915.
44. Alecci M, Penna SD, Sotgiu A, Testa L, Vannucci I. Electron paramagnetic resonance spectrometer for three-dimensional in vivo imaging at very low frequency. Rev Sci Instrum 1992; 63:4263–4270.
45. Sotgiu A, Alecci M, Brivati J, Placidi G, Testa L. New experimental modalities of low frequency electron paramagnetic resonance imaging. In: Ohya-Nishiguchi H, Packer L, editors. Bioradicals detected by ESR spectroscopy. Basel: Birkhauser Verlag; 1995. p 69–92.

46. Quine RW, Eaton GR, Eaton SS. Pulsed EPR spectrometer. Rev Sci Instrum 1987; 58:1709–1724.
47. Quine RW, Rinard GA, Ghim BT, Eaton SS, Eaton GR. A 1–2 GHz pulsed and continuous wave electron paramagnetic resonance spectrometer. Rev Sci Instrum 1996; 67:2514–2527.
48. Rinard GA, Quine RW, Harbridge JR, Song R, Eaton GR, Eaton SS. Frequency dependence of EPR signal-to-noise. J Magn Reson 1999; 140:218–227.
49. Rinard GA, Quine RW, Eaton SS, Eaton GR. Frequency dependence of EPR signal intensity. 248 MHz to 1.4 GHz. J Magn Reson 2002; 154:80–84.
50. Froncisz W, Camenisch TG, Ratke JJ, Hyde JS. Pulse saturation recovery, pulse ELDOR, and free induction decay electron paramagnetic resonance detection using time-locked subsampling. Rev Sci Instrum 2001; 72: 1837–1842.
51. Rinard GA, Quine RW, Eaton SS, Eaton GR, Froncisz W. Relative benefits of overcoupled resonators vs. inherently low-Q resonators for pulsed magnetic resonance. J Magn Reson A 1994; 108:71–81.
52. Rinard GA, Quine RW, Song R, Eaton GR, Eaton SS. Absolute EPR spin echo and noise intensities. J Magn Reson 1999; 140:69–83.
53. Ardenjaer-Larsen JH, Laursen I, Leunbach I, Ehnholm G, Wistrand L-G, Petersson JS, Golman K. EPR and DNP properties of certain novel single electron contrast agents intended for oximetric imaging. J Magn Reson 1998; 133:1–12.
54. Quine RW, Harbridge JR, Eaton SS, Eaton GR. Design of a programmable timing unit. Rev Sci Instrum 1999; 70:4422–4432.
55. Quine RW. Programmable timing unit for generating multiple coherent timing signals. US Patent 5,621,705; 1997.
56. Quine RW. Programmable timing unit for generating multiple coherent timing signals. US Patent 5,901,116; 1999.
57. Quine RW, Rinard GA, Eaton SS, Eaton GR. EPR resonator coupling monitor. J Magn Reson 1992; 99: 571–575.
58. Quine RW, Eaton GR. Setting the microwave phase in an EPR spectrometer. J Magn Reson A 1996; 119:268–270.
59. Rinard GA, Quine RW, Eaton GR, Eaton SS. Adapting a Hall probe controller for current control of an air-core magnet. Concepts Magn Reson 2002; 15:59–62.
60. Rinard GA, Quine RW, Eaton GR, Eaton SS, Barth ED, Pelizzari CA, Halpern HH. Magnet and gradient coil system for low-field EPR imaging. Concepts Magn Reson 2002; 15:63–70.
61. Eaton GR, Quine RW. Comparison of four digitizers for time-domain EPR. Appl Spectros 2000; 54:1543–1545.